AWARD NUMBER: W81XWH-19-1-0378

TITLE: Combining Androgen Deprivation and Immunotherapy to Prevent Progression to Castration-Resistant Prostate Cancer

PRINCIPAL INVESTIGATOR: Kent L. Nastiuk, Ph.D.

CONTRACTING ORGANIZATION: Health Research-Roswell Park Cancer
Buffalo, NY

REPORT DATE: October 2022

TYPE OF REPORT: Annual

PREPARED FOR: U.S. Army Medical Research and Development Command
Fort Detrick, Maryland 21702-5012

REPORT DOCUMENTATION PAGE

Form Approved
OMB No. 0704-0188

1. REPORT DATE	2. REPORT TYPE	3. DATES COVERED
October 2022	Annual	01Sep2021-31Aug2022

4. TITLE AND SUBTITLE

Combining Androgen Deprivation and Immunotherapy to Prevent Progression to Castration-Resistant Prostate Cancer

5a. CONTRACT NUMBER
W81XWH-19-1-0378

5b. GRANT NUMBER
PC180278

5c. PROGRAM ELEMENT NUMBER

6. AUTHOR(S)
Kent L. Nastiuk, PhD

E-Mail: kent.nastiuk@roswellpark.org

5d. PROJECT NUMBER

5e. TASK NUMBER

5f. WORK UNIT NUMBER

7. PERFORMING ORGANIZATION NAME(S) AND ADDRESS(ES)

Health Research, Inc.
Health Research-Roswell Park
Cancer Inst
Elm and Carlton St
Buffalo NY 14263-0001

8. PERFORMING ORGANIZATION REPORT

9. SPONSORING / MONITORING AGENCY NAME(S) AND ADDRESS(ES)

U.S. Army Medical Research and Development Command
Fort Detrick, Maryland 21702-5012

10. SPONSOR/MONITOR'S ACRONYM(S)

11. SPONSOR/MONITOR'S REPORT NUMBER(S)

12. DISTRIBUTION / AVAILABILITY STATEMENT

Approved for Public Release; Distribution Unlimited

13. SUPPLEMENTARY NOTES

14. ABSTRACT

Recently, we found that in a PTEN-deficient mouse PCa model, castration induces an immunosuppressive state within the tumor that is concurrent with tumor recurrence. Mechanistically, this response to ADT is mediated by soluble mediators (TNF and CCL2), facilitating communication between tumor, stromal and immune cell populations within the tumor microenvironment. Based on these preliminary data, we hypothesize: Blocking myeloid suppression prevents progression to castration resistant prostate cancer. We test this hypothesis in three aims. Aim 1 examines the mechanism of paracrine TNF signaling between tumor, stromal and myeloid cell populations within the TME, in inducing immune suppression following ADT. Aim 2 tests whether blocking the transit and/or function of myeloid suppressive cell populations prevents CRPC (tumor recurrence following ADT). We also determine the role of PTEN in ADT-induced immune evasion. Aim 3 tests the hypothesis that ADT, in men with locally advanced PrCa, increases serum TNF and CCL2, as well as circulating myeloid cells, by assessing samples from an ongoing clinical study.

15. SUBJECT TERMS
androgen, castration, immunotherapy, prostate, cancer, TNF, CCL2, tumor associated macrophages, CD8 T-cells

16. SECURITY CLASSIFICATION OF:			17. LIMITATION OF ABSTRACT	18. NUMBER OF PAGES	19a. NAME OF RESPONSIBLE PERSON
a. REPORT	b. ABSTRACT	c. THIS PAGE			USAMRDC
Unclassified	Unclassified	Unclassified	Unclassified	52	19b. TELEPHONE NUMBER *(include area code)*

TABLE OF CONTENTS

1. INTRODUCTION:

Most prostate cancer (PCa) deaths are due to castration resistant PCa (CRPC). While androgen deprivation therapy is the standard of care for patients with advanced PCa, nearly universal progression to CRPC occurs 2-3 years after ADT is initiated. Although there have been key advances in the treatment of CRPC, even the best therapies are not curative. One approach to this problem is to improve the initial treatment of advanced prostate cancers, by combining complementary therapies with ADT, to prevent progression of such advanced cancers to CRPC. Immunotherapy, typically employing T-cell 'checkpoint' inhibitors, has provided very durable remissions, verging on cure for a variety of cancer types. However, CPIs have *not* been effective in prostate cancers, perhaps because such cancers are 'cold' (lacking cytolytic CD8 T-cells). Cold tumors may be caused by infiltration of myeloid cell populations – tumor associated macrophages (TAMs) and myeloid-derived suppressor cells (MDSCs) – into the tumor immune cell microenvironment (TIME). In preliminary data accompanying this proposal, we demonstrate that castration of a PTEN-deficient mouse PCa model induces an immunosuppressive state within the tumor that is concurrent with the onset of tumor recurrence. The response to castration/ADT is tri-phasic: a pro-apoptotic regression phase where tumor shrinks, followed by selection for a residual population of resistant stem-like tumor cells and finally recurrent growth as CRPC. Using PCa cell lines to model the first two phases of the response to ADT, we have shown that ADT induces apoptosis, thereby enriching for an ADT-resistant stem/progenitor population that we demonstrate is an *in vitro* source of enhanced TNF production. Mechanistically, in our model system the response to ADT is driven by the soluble mediators TNF and CCL2, which facilitate communication within the TIME. Specifically, a TNF-CCL2-CCR2 paracrine loop is induced between prostate cancer cells and non-tumor cells in the microenvironment: TNF produced by tumor cells acts on myofibroblasts and TAMs to induce CCL2 production, which in turn recruits tumor-associated macrophages (TAMs) and possibly MDSCs. Analysis of public PCa data sets shows TNF and stem/progenitor marker expression are both increased in CRPC, consistent with our hypothesis that ADT drives the development of an immuno-suppressive state via a cytokine switching mechanism that triggers the TNF-CCL2-CCR2 axis in the TIME.

2. KEYWORDS:

androgen, castration, immunotherapy, prostate, cancer, TNF, CCL2, tumor associated macrophages, CD8 T-cells, myeloid-derived suppressor cells, CCR2, TNF receptors, tumor microenvironment

3. ACCOMPLISHMENTS:

What were the major goals of the project?

We proposed that TNF promotes an immunosuppressive state via CCL2, to drive castration-resistant tumor growth.

- Aim 1 determines the role of tumor-microenvironment-derived TNF as a trigger to induce vascular regression following ADT.

- Aim 2 tests our immune suppression hypothesis in three sub-aims.

- Aim 3 tests the hypothesis that ADT administered to men with locally advanced PCa increases serum TNF and CCL2

What was accomplished under these goals?

Accomplished under Aim 1:

We completed the remainder of Aim 1 (revised Major Task 2 and revised Major Task 3). The results of these investigations have now been published (see Appendix)

Accomplished under Aim 2

We completed the proposed tasks.

Major Task 1: Determine if therapies directed against TNF and/or CCL2 signaling will prevent castrate resistant recurrence. This provides information on whether or not these soluble mediators are acting in as part of a signaling cascade and complements the insight from Aim 1.

Major Task 2: Determine whether therapies in sub-aim 1 inhibit immune suppression. This key sub-aim determines if immune suppression is the driving force behind recurrence.

Major Task 3: assess hi-MYC model. The purpose is to determine if castration induced immune suppression enhances recurrence in a second model of prostate cancer.

The results are detailed below:

To investigate the response of prostate cancer to androgen deprivation therapies, we examined mice engineered to delete the PTEN gene in the prostate epithelium at puberty uniformly develop an intraductal form of prostate adenocarcinoma (Table 1) used high frequency ultrasound (HFUS) and three-dimension reconstruction software to serially determine the volume of tumors in live animals (Figure 1A). As seen in Figure 1B, the kinetics of tumor volume following castration is complex. Immediately following castration, tumor volume continues to increase similar to the non-castrated control. We recently demonstrated that this regression delay (normal prostate starts regressing immediately following castration) is driven by glucocorticoid receptor signaling transiently substituting for AR signaling. Following this delay, the tumors regressed as expected but within ~5 weeks most began to increase in volume, implying tumor recurrence and mimicking the development of CRPC in men.

Table 1. Genetically-engineered murine models of prostate cancer used in these studies

Mouse genotype (common name)	PB-Cre4 x PTEN$^{f/f}$ (Pten-deficient)	ARR$_2$PB-*MYC* (Hi-MYC)
Mouse background	C57Bl/6:129SvJ	FVB
Primary murine lobe	Anterior prostate	Ventral prostate
H&E histology	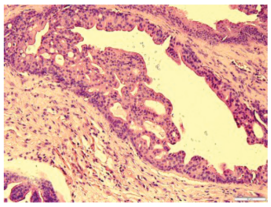 Intraductal histology infrequent in human PrCa	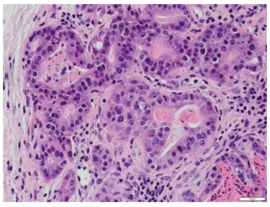 acinar histology most common human PrCa
Mouse age when tumor volume is ~300-500 mm^3	~ 6 months	~ 10 months

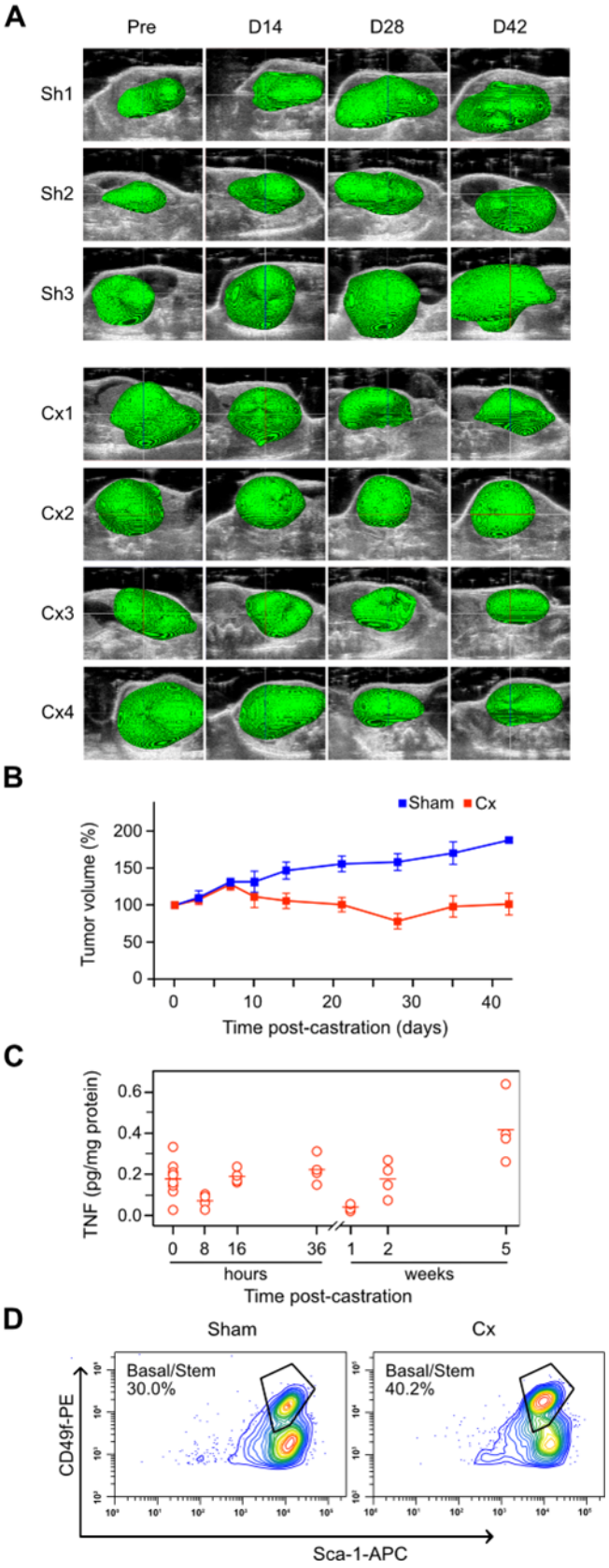

Figure 11. Castration induces tumor recurrence, and an increase in TNF and stemness in prostate tumors from PTEN-deficient mice.

Mice bearing PTEN-deficient tumors were either castrated (Cx1-4) or sham-operated (Sh1-3) and serially imaged using HFUS. In some cases, tumor tissue was recovered for further analysis. **A**. 3D reconstruction of tumor-bearing ventral lobes (pseudo-colored green) performed as described in Materials & Methods. **B**. Tumor volume kinetics post-castration. Tumor volume was determined from HFUS images using Amira software. Mean tumor volume at the indicated times post-castration (n=4, red) or post-sham operation (n=3, blue) is shown as percent pre-castration volume (mean [%] ± SEM). **C**. TNF levels in tumors tissue extracts were measured by ELISA and normalized to total protein in the tissue sample, at the indicated times post castration. **D**. LSC FACS analysis of tumor cells from sham (left) and castrated (Cx; right) PTEN-deficient mice. Tumors were disaggregated and cells were processed for Lin^-/Sca-1/CD49f FACS analysis (200). Relative fluorescence intensities are shown as contour plots. The LSC^{hi} population is labeled 'Basal/stem'. The population in the lower right quadrant (LSC^{med}) corresponds to luminal progenitors. A representative analysis is shown. Sham LSC FACS was replicated 5 times (mean[%]±SEM = 27.0±4.0); 25d post-castration LSC FACS was replicated 4 times (mean[%]±SEM = 38.2±1.7).

We measured TNF protein levels in tumor lysates, and found an increase at 5 weeks post-castration, when tumor recurrence is beginning (Figure 1C). Previously, we had observed an increase in *Tnf* mRNA at 8 hours post-castration in the stromal compartment of the normal prostate, suggesting a relatively direct effect of androgen-withdrawal on TNF expression. In the case of PTEN-deficient tumors, the increase in TNF protein at a late time post-castration suggests a more complex transcriptional and/or translational regulatory mechanism in response to androgen withdrawal. Alternately, the increase in TNF at late times post-castration might be due to the expansion of a population of TNF-expressing cells as the tumor evolves in response to androgen deprivation. We queried gene expression profiles in public databases from two previously published studies of men who had either hormone-naïve PC or CRPC, to gain insight into this question. Increased *TNF* mRNA expression in CRPC, relative to castration-naive primary PC, correlated with elevated expression of various stem cell-related genes in both datasets (Figure 2).

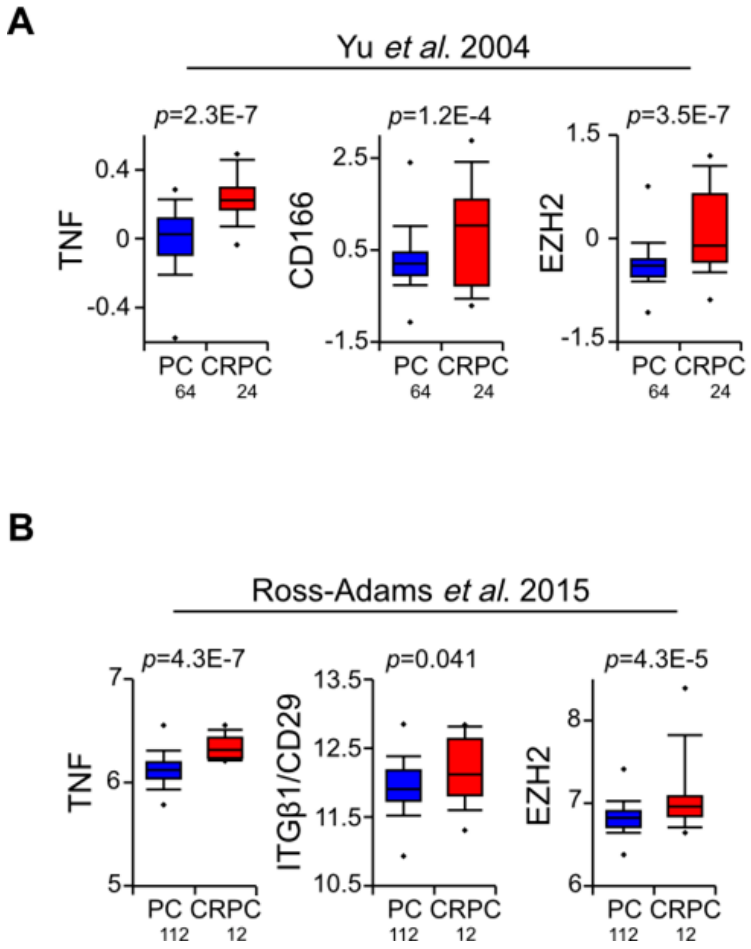

Figure 2. Expression of basal/stem cell related genes and TNF in human prostate cancer samples. A. TNF and **stem cell markers** mRNA expression in human primary PC (blue) and CRPC (red) from the indicated publications, extracted and analyzed at the Oncomine.org (**A**) or GEO (**B**) web browsers, and plotted as box and whisker plots. Sample size (bottom) and p-value (top) are indicated. PC and CRPC sample sets were compared by Student's unpaired *t*-test. We previously reported the TNF expression analysis (in the left-most part of panel A) of the Yu et al. 2004 dataset in a separate set of correlative gene expression analyses).

Androgen-deprivation induced TNF secretion is due to increased basal cell stemness.

To determine if we could detect a change in the stem cell-like tumor epithelial cell populations as the tumors began to increase in volume following castration-induced regression, we examined single cell preparations from tumors for cell surface expression of stem cell markers, using fluorescent-activated cell sorting (FACS). We observed an increase in $Lin^-/Sca1^+/CD49f^{hi}$ (LSC^{hi}) cells at 25 days post-castration, relative to non-castrated tumors (Figure 1D). These cells correspond to the $cytokeratin\text{-}5^+/p63^+$ basal stem cell population, a multipotent stem cell population that is required for the post-natal development of the prostate. Basal stem cells are distinct from $Lin^-/Sca1^+/CD49f^{med}$ (LSC^{med}) luminal progenitor cells (identified in the lower right population in Figure 3D) that are the likely tumor initiating cell populations for most human prostate cancers.

The data in Figures 1 and 2 suggest that the TNF secreted during the post-castration recurrence phase in the PTEN-deficient tumors might be derived from a basal stem cell population. To test this more thoroughly, we performed experiments using the C4-2 and LNCaP cell culture models of PC. First, we observed that long-term culture in the anti-androgen enzalutamide significantly reduced the growth rate of C4-2 prostate cancer cells (Figure 3A), as expected. Reduced growth was accompanied by an increase in the fraction of cells that resembled basal stem cells (Figure 3B-C) and a coordinate increased in TNF levels (Figure 3C). In the analyses for Figure 33, we employed CD166 as a basal stemness biomarker. We also performed the enzalutamide selection experiment on the LNCaP cell line, which is the isogenic parental line for C4-2, and is more androgen-responsive (Figure 4A). We observed a similar correlation between stemness and TNF secretion (Figure 4B-C).

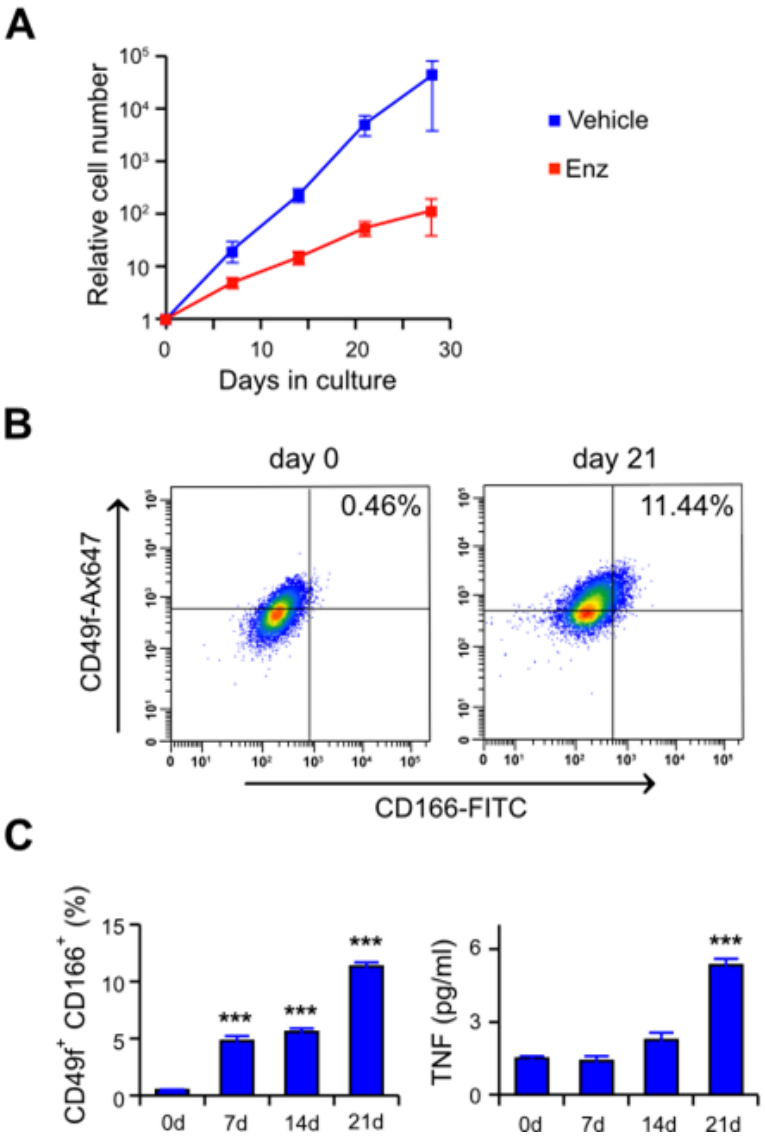

Figure 3. **Extended enzalutamide treatment selects for basal stemness and TNF secretion.** C4-2 cells were grown in media plus 10% serum and treated with vehicle (blue) or 10 μM enzalutamide (Enz; red) for the indicated time. **A.** C4-2 cell growth curve in the presence of enzalutamide. Cells were counted microscopically at the indicated times. Data are shown as mean ± s.e.m. (n=3). **B.** FACS analysis for basal cell stemness markers in enzalutamide treated C4-2 cells. Cells grown in enzalutamide for the indicated time, were incubated with the fluor-labeled antibodies, analyzed by FACS and relative fluorescence intensity represented as dot plots. The fraction of the cells that correspond to the $CD49f^{hi}/CD166^{hi}$ population (upper, right quadrant) is indicated. Additional time points are in Figure 34. **C.** Fraction of cells scoring $CD49f^{hi}/CD166^{hi}$ and corresponding TNF secretion, at the indicated time of culture in media plus enzalutamide. Data from FACS analyses (see Figure 34) is plotted on the left and TNF levels in the media determined by ELISA is plotted on the right. Values are given as mean ± s.e.m. (n = 2). **, $p < 0.01$ ***$p < 0.001$ (two-way ANOVA followed by Tukey-Kramer HSD test).

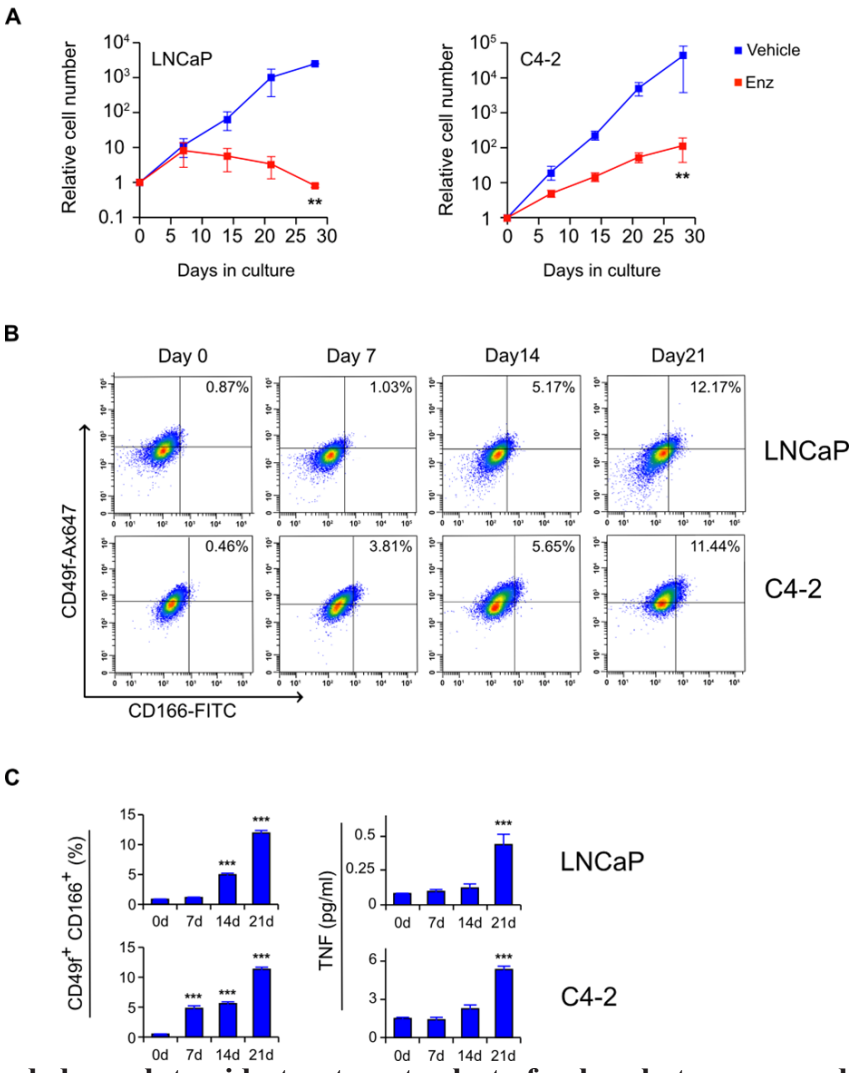

Figure 42. Extended enzalutamide treatment selects for basal stemness and TNF secretion: extended version of Figure 3. This figure is an expanded version of Figure 3, with reproduction of the C4-2 data from Figure 33, plus additional results from similar experiments using LNCaP, a more androgen-dependent cell line that is the parental cell line for C4-2. C4-2 or LNCaP cells were grown in media plus 10% serum and treated with vehicle (Vehicle; blue) or 10 μM enzalutamide (Enz; red) for the indicated time. **A.** LNCaP (left) and C4-2 (right) cell growth curve in the presence of enzalutamide. Cells were counted microscopically at the indicated times. Data are shown as mean ± s.e.m. (n=3). **B.** FACS analysis for basal cell stemness markers in enzalutamide treated LNCaP (upper row) and C4-2 (lower row) cells. Cells grown in enzalutamide for the indicated time were incubated with the indicated fluor-labeled antibodies and analyzed by FACS. The relative fluorescence intensity is represented as dot plots. The fraction of the cells that correspond to the $CD49f^{hi}/CD166^{hi}$ population (upper, right quadrant) is indicated. **C.** TNF secretion and corresponding Fraction of cells scoring $CD49f^{hi}/CD166^{hi}$ and corresponding TNF secretion. Data from FACS analyses (panel **B**) is plotted on the left and TNF determined by ELISA is plotted on the right. Values are given as mean ± s.e.m. (n = 2). **, $p < 0.01$ ***$p < 0.001$ (two-way ANOVA followed by Tukey-Kramer HSD test

Finally, we replicated enzalutamide selection for both C4-2 and LNCaP cell lines, using immunofluorescence microscopy to identify CD49f^{hi} and CD166^{hi} cells (Figure 5). Again, an increase in the fraction of cells scoring for these basal stemness markers correlated with increased TNF secretion. Stem cell marker enrichment >10% was typically required to detect an increase in TNF in the media of enzalutamide-treated cultures.

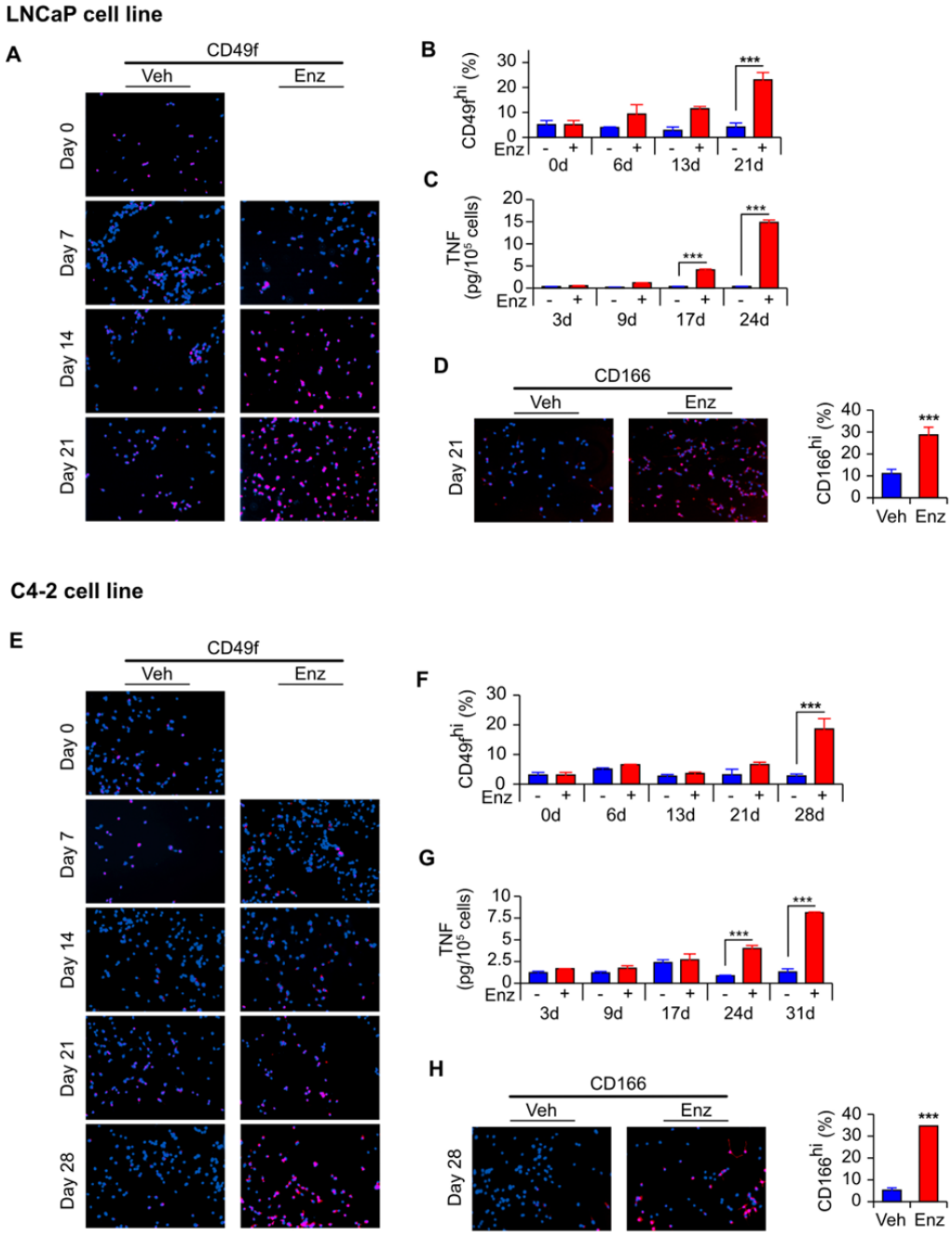

Figure 5. Extended enzalutamide treatment selects for basal stemness and TNF secretion: immunofluorescence staining of basal markers CD49f and CD166. LNCaP and C4-2 cells were treated with vehicle (–, blue) or 10 μM enzalutamide (Enz; +, red) for the indicated time. Aliquots of the corresponding cultures were incubated with either anti-CD49f or anti-CD166 antibodies, followed by appropriate fluorescent-tagged secondary antibodies. Hoechst stain was used to identify nuclei. Representative photomicrographs were captured under appropriate fluorescence and fluorescent cells counted. **Panels A-D.** LNCaP cell line. Fluorescent microscopic images corresponding to CD49f (**A**) and CD166 (**D**, left side) following the indicated treatments. The corresponding quantitation is plotted for CD49f (**B**) and CD166 (**D**, right side). The TNF levels, determined by ELISA of the media for the indicated cultures (**C**). Plotted values are given as mean ± s.e.m. of percentage of positively stained cells ($n = 3$). ***$p<0.001$(Two-way ANOVA followed by Tukey-Kramer HSD test). **Panels E-H.** C4-2 cell line. Analogous to those shown for LNCaP in panels **A-D**.

Next, we treated C4-2 cells with enzalutamide for 20 days and used preparative FACS to partially purified cells into $CD166^{lo}$ and $CD166^{hi}$ fractions (Figure 6A). TNF levels were higher in conditioned media from the $CD166^{hi}$ fraction relative to the $CD166^{lo}$ fraction (Figure 6B). We also demonstrated that the efficiency of colony formation – a functional marker of stemness – correlated with the level of expression of CD166 (Figure 6C).

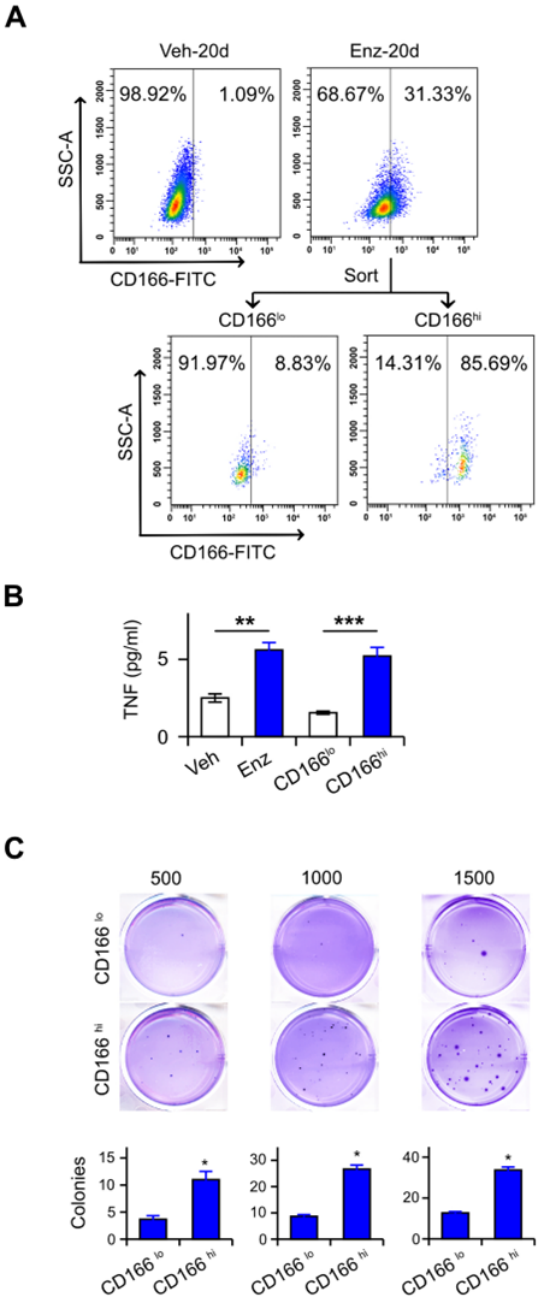

Figure 6. Enzalutamide treatment selects for a TNF-expressing basal stem cell population. C4-2 cells were grown for 20 days in media plus 10% serum containing 10 μM enzalutamide, enriched for CD166^{hi} expression. ELISA was used to measure TNF and colony formation. **A.** CD166-enrichment was performed via FACS to sort CD166^{hi} and CD166^{lo} C4-2 cells treated as indicated. The purity of the unsorted and sorted CD166^{hi} and CD166^{lo} populations are shown. **B.** TNF secretion of the indicated cultures (left to right): unsorted, vehicle-treated (veh); unsorted, enzalutamide-treated (enz); and sorted, enzalutamide-treated (CD166^{lo}, CD166^{hi}). TNF measured by ELISA, and plotted as mean ± s.e.m. (n=3). $^{**}p<0.01$, $^{***}p<0.001$ (One-way ANOVA followed by Tukey-Kramer HSD test). **C.** Colony formation assay of enriched CD166^{hi} and CD166^{lo} cell populations sorted as in **A**. Seeding densities were 500, 1000, and 1500 cells/well, respectively. Colony counts per well are plotted. $^{*}p<0.05$ (Student's unpaired *t*-test).

Differentially-timed blockade of TNF signaling.

We previously employed cell culture and mouse models of prostate cancer to demonstrate that TNF signaling mediates two distinct responses to ADT – an anti-tumorigenic apoptotic/regression phenotype and a pro-tumorigenic cell migration phenotype. Given the observations in Figure 1, we hypothesized that TNF mediates both the regression and recurrence phases that occur after castration (Figure 1B). To test this, we treated tumor-bearing mice with etanercept – a TNFR2-Fc fusion protein, which competitively binds TNF and prevents receptor binding – at three time points: three days prior, one day prior, and three days following castration. When etanercept is administered three days before castration (Figure 7A, -3d), castration-induced regression is blocked, and tumor growth is similar to the sham group (Figure 1B). Etanercept given one day before castration, does not affect regression but blocks recurrence (Figure 7A, -1d). Finally, when etanercept was administered three days after castration there is no detectable effect on regression or recurrence (Figure 7A, +3d). Instead, the result resembles castration alone (Figure 1B).

To gain insight into the nature of the different molecular processes occurring during regression and recurrence, we performed gene set enrichment analysis (GSEA) on RNA sequence data from bulk tumor mRNA. Specifically, we compared samples from sham castrated mice with those from either mice six days after castration (Figure 7B, upper panel) or mice 35 days after castration (Figure 7B, lower panel). Multiple gene sets related to TNF-induced transcription, most NFkB-related, were uniformly down-regulated at six days post-castration but up-regulated 5 weeks after castration, relative to the sham conditions. The switch in TNF-related gene sets from down-regulation to up-regulation is consistent with a switch from apoptosis signaling (low NFkB levels) to signaling that promotes transcription of NFkB-regulated genes (high NFkB levels).

A

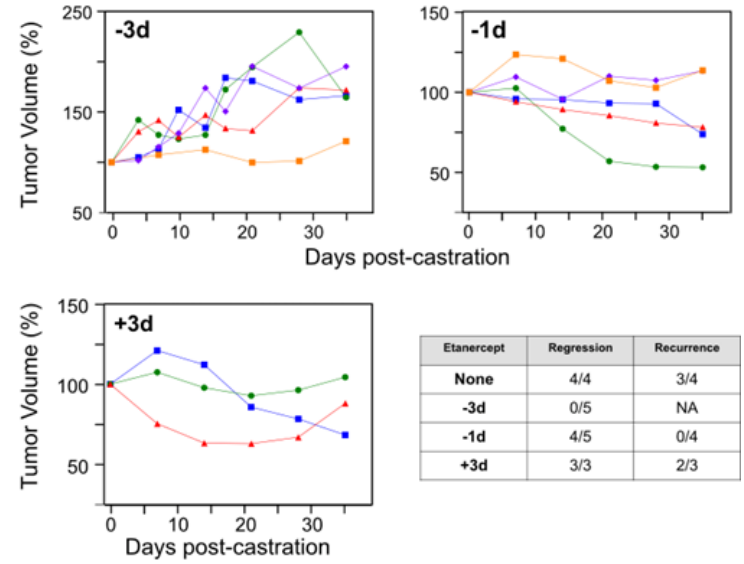

Etanercept	Regression	Recurrence
None	4/4	3/4
-3d	0/5	NA
-1d	4/5	0/4
+3d	3/3	2/3

B

Sham vs CX_6d

Genesets	SIZE	NES	p.val	FDR
PHONG_TNF_RESPONSE_VIA_P38_PARTIAL	144	-2.98	<0.01	5.16E-05
PHONG_TNF_RESPONSE_VIA_P38_COMPLETE	208	-2.94	<0.01	5.65E-05
RUAN_RESPONSE_TO_TNF_TROGLITAZONE_DN	39	-2.70	<0.01	2.97E-04
PHONG_TNF_TARGETS_UP	60	-2.65	<0.01	3.72E-04
RUAN_RESPONSE_TO_TNF_DN	80	-2.62	<0.01	4.81E-04
ZHOU_TNF_SIGNALING_30MIN	51	-1.97	<0.01	2.35E-02
ZHANG_RESPONSE_TO_IKK_INHIBITOR_AND_TNF_UP	190	-1.88	0.01	3.52E-02
ZHOU_TNF_SIGNALING_4HR	49	-1.85	0.01	4.09E-02
WANG_TNF_TARGETS	18	-1.77	0.02	5.82E-02
RUAN_RESPONSE_TO_TNF_TROGLITAZONE_UP	15	-1.68	0.03	8.09E-02

Sham vs CX_35d

Genesets	SIZE	NES	p.val	FDR
ZHANG_RESPONSE_TO_IKK_INHIBITOR_AND_TNF_UP	193	3.96	<0.01	9.35E-06
PHONG_TNF_TARGETS_UP	61	3.96	<0.01	9.35E-06
PHONG_TNF_RESPONSE_NOT_VIA_P38	307	3.72	<0.01	9.35E-06
WANG_TNF_TARGETS	19	3.5032	<0.01	9.35E-06
TIAN_TNF_SIGNALING_VIA_NFKB	27	3.2884	<0.01	9.35E-06
TIAN_TNF_SIGNALING_NOT_VIA_NFKB	21	2.7396	<0.01	1.64E-04
SANA_TNF_SIGNALING_UP	65	2.7088	<0.01	2.21E-04
PHONG_TNF_RESPONSE_VIA_P38_PARTIAL	149	2.3381	<0.01	2.27E-03
SANA_TNF_SIGNALING_DN	82	2.1602	<0.01	6.18E-03
ZHOU_TNF_SIGNALING_30MIN	51	1.8286	<0.01	3.32E-02
ZHOU_TNF_SIGNALING_4HR	49	1.7752	0.02	4.19E-02

Figure 73. Differentially-timed TNF signaling blockade has distinct effects on tumor growth. Mice with PTEN-deficient tumors were castrated and etanercept (sTNFR2-Fc) was administered at the indicated times: three days before (-3d), one day before (-1d), or three days after (+3d) surgical castration. **A.** Tumor volume kinetics. Tumor volumes were determined by serial HFUS imaging and 3D reconstruction and plotted after normalizing to the initial tumor volume for each mouse. Different colors/symbols represent individual mice. The table summarizes regression and recurrence incidence for each experiment. Growth curves for castrated mice that did not receive etanercept (None) are not shown. The criteria for regression and recurrence are described in the Methods. **B.** Gene set enrichment analysis. RNA was extracted from PTEN-deficient tumors from the following mice: sham-operated, 6d post-castration and 35d post-castration. GSEA was performed on bulk RNA-seq data using gene sets corresponding to TNF-related pathways. Normalized enrichment scores (NES) from 6d (down-regulated, blue) and 35d (up-regulated, red) post-castration were compared to the sham group. Gene sets common to the two analyses are yellow.

CCL2 signaling is required for castration-resistant recurrence of murine prostate cancer models. CCL2 is chemotactic cytokine (chemokine) (214) linked to prostate cancer pathogenesis. The CCL2-CCR2 signaling axis has multiple pro-tumorigenic functions, most notably the recruitment and polarization of tumor associated macrophages (TAMs). Previously we demonstrated autocrine CCL2 secretion following enzalutamide induction of TNF in mono-cultures of C4-2 cells, consistent with CCL2 gene transcription via TNF induction of NFkB. We returned to the enzalutamide selection experiments shown in Figure 3 and Figure 4 and found that the secretion of CCL2 protein increased over time, coordinately with TNF secretion, in enzalutamide treated C4-2 and LNCaP cells (Figure 8A). To assess paracrine CCL2 production in response to androgen deprivation, we replicated these experiments using co-cultures of LNCaP or C4-2 plus the myofibroblast-like WPMY-1 cell line, grown in enzalutamide-containing media. Again, we observed coordinate secretion of TNF and CCL2 (Figure 8B). Co-cultures produced 5- to 20-fold more CCL2 than the prostate cancer cell line mono-cultures. We also found that enzalutamide-treated co-cultures of C4-2 plus WPMY-1 produced conditioned media that induced migration of THP-1, a $CCR2^{+}$ macrophage-like leukemia cell line that is a model for TAMs.

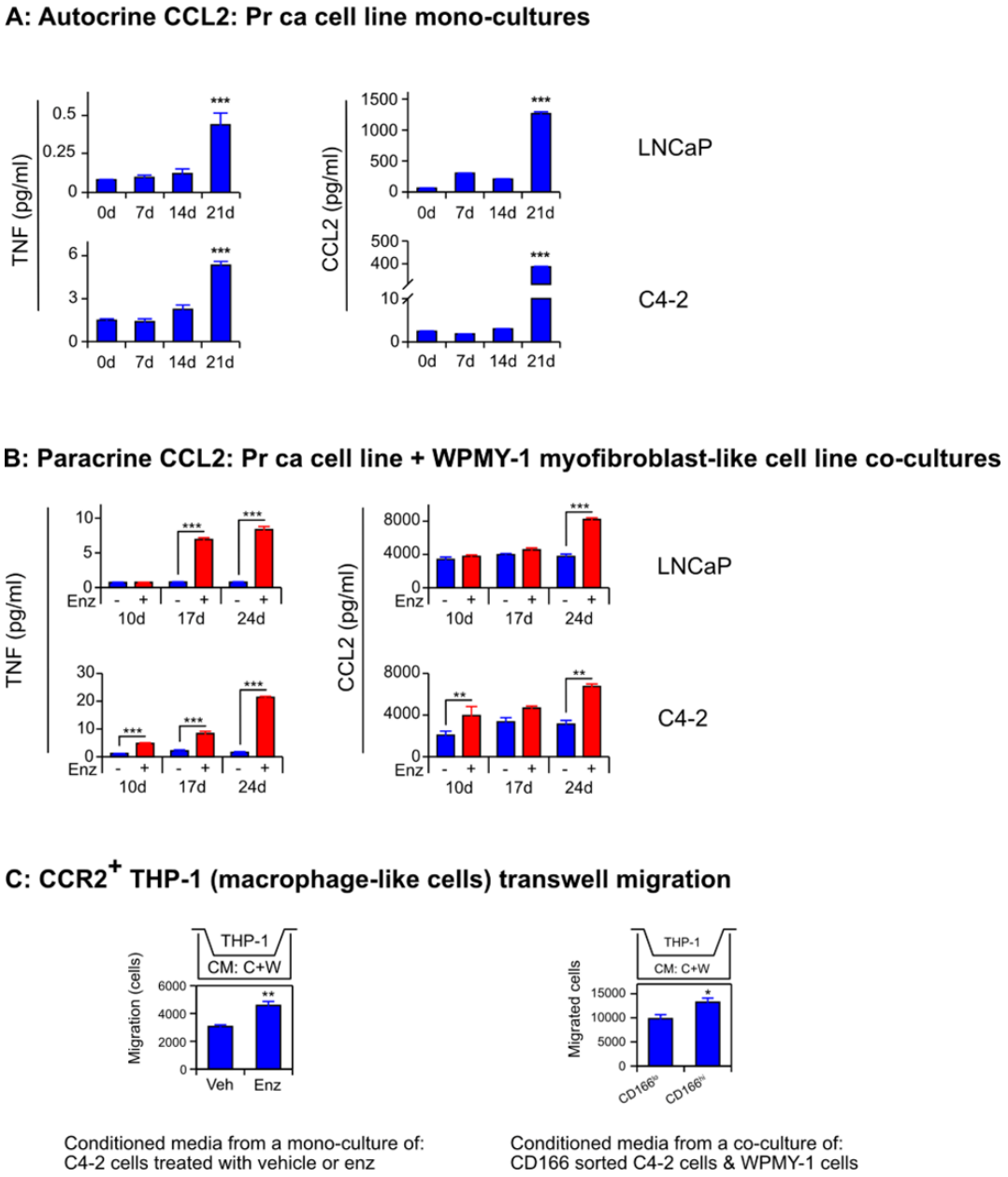

Figure 8 Enzalutamide induces CCL2 secretion under autocrine and paracrine conditions. A. Autocrine CCL2 production by LNCaP and C4-2 mono-cultures. The TNF ELISA data is reproduced from Figure 33C. The CCL2 ELISA data is from the same cultures. **B.** Paracrine CCL2 production by prostate cancer cell lines (LNCaP and C4-2) co-cultured with WPMY-1 myofibroblasts. TNF and CCL2 were assayed by ELISA using the media from cultures treated as indicated. For panels **A** and **B**, values are given as mean ± s.e.m. ($n = 2$). **, $p < 0.01$ ***$p < 0.001$ (Two-way ANOVA followed by Tukey-Kramer HSD test). **C.** Migration of THP-1 macrophage-like cells towards conditioned media from enzalutamide treated co-cultures. As diagrammed, transwell analysis of THP-1 migration, toward conditioned media from C4-2/WPMY-1 co-cultures (CM: C+W). Left: co-cultures were treated as indicated. Right: Live C4-2 cells sorted into $CD166^{lo}$ and $CD166^{hi}$ fractions as described in Figure 36A, then separately co-cultured with WPMY-1 cells. Data are given as mean ± s.e.m. ($n = 3$), *p<0.05, **p<0.01, ***p<0.001 (Student's unpaired t-test).

These observations suggested that paracrine TNF induction of CCL2 in the prostate cancer TME might be responsible for tumor recurrence at late times post-castration, possibly by recruiting immunosuppressive TAMs. Indeed, we found that in the samples from Figure 1C, CCL2 increased at 5 weeks (Figure 9A), coincident with the rise in TNF that accompanies tumor recurrence. Tissue sections corresponding to tumors 5 weeks post-castration showed an increase in stroma-localized macrophage-like cells expressing CCL2 (Figure 9B). Moreover, CCL2 expression was reduced in tumor tissue sections from castrated mice that received etanercept, consistent with CCL2 regulation by TNF (Figure 9B). To determine if CCL2 signaling was necessary for post-castration tumor recurrence in prostate cancer mouse models, mice bearing PTEN-deficient prostate cancers received an antagonist of CCR2 (BMS-741672; CCR2a) prior to castration. Serial imaging revealed that none of the tumors recurred (Figure 9C), indicating that CCL2-CCR2 signaling is indeed required for castration resistant recurrence in this model. Importantly, the tumor kinetics produced by CCR2 blockade phenocopies the effect of etanercept administered one-day prior to castration (Figure 7A, -1d), consistent with TNF regulation of CCL2 gene transcription via NFkB. To confirm the role of CCL2 signaling we replicated the CCR2 inhibition studies in the Hi-MYC prostate cancer GEMM, which has a similar response to castration (regression delay, regression then recurrence) as the PTEN-deficient GEMM (Figure 9D, blue symbols). We observed that CCR2a treatment prior to castration was comparably effective at inhibiting castration-resistant recurrence in Hi-MYC mice (Figure 9D, red symbols; Figure 10).

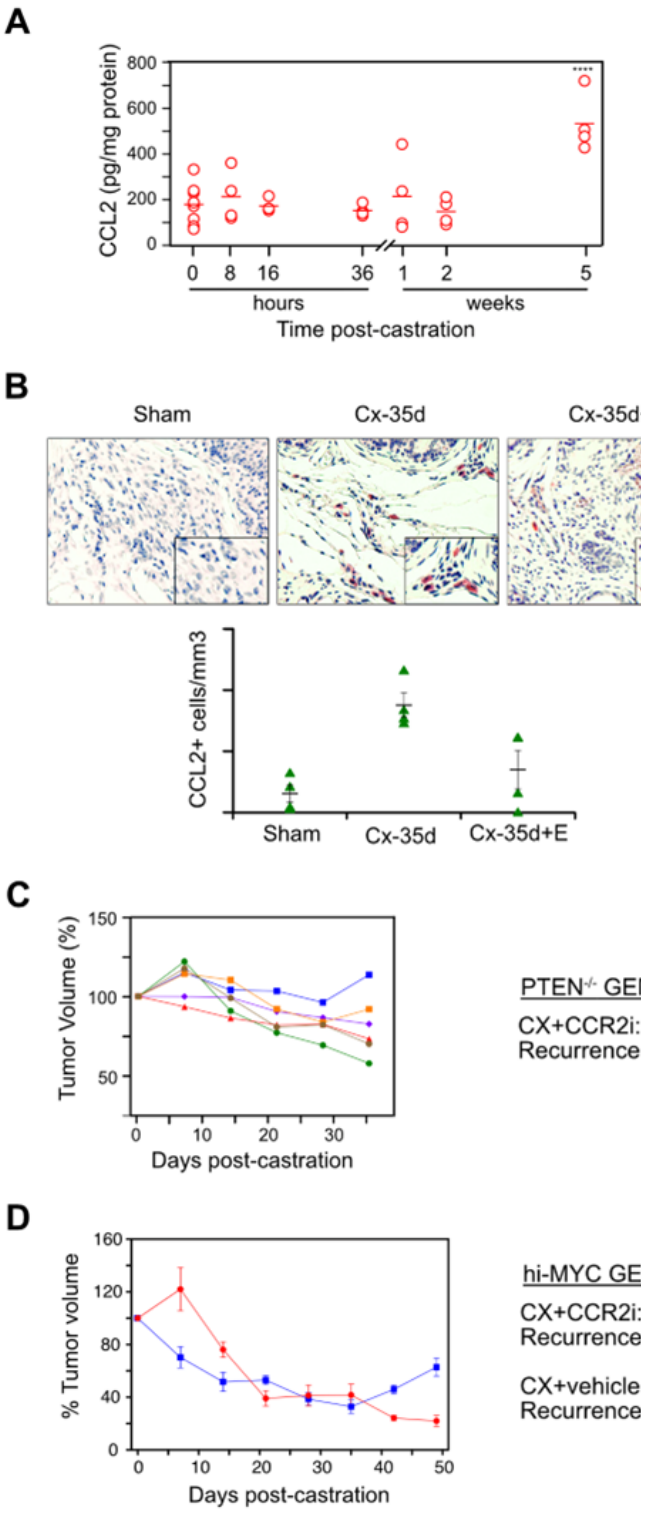

Figure 9. CCL2-CCR2 signaling is required for castration-resistant recurrence. Mice bearing PTEN-deficient (**A-C**) or hi-MYC (**D**) tumors were sham-operated or castrated at the indicated times. Volume was monitored by HFUS. Some mice received etanercept or the CCR2i, as indicated. **A**. Tumor CCL2 levels following castration. CCL2 levels were measured by ELISA on the same tumor extracts prepared for Figure 31C, normalized to total protein and plotted. The bar marks the mean. ****$p <$ 0.0001 (Two-way ANOVA followed by Tukey-Kramer HSD test). **B.** Representative images of IHC-stained $CCL2^{+}$ cells (red) in tumors from the indicated treatment groups. CCL2+ cells were counted and plotted. **C.** Treatment with a CCR2 antagonist phenocopies -1d etanercept treatment (Figure 37A) in PTEN-deficient tumor-bearing mice. Tumor volumes were determined by serial HFUS imaging and 3D reconstruction and plotted after normalizing to the initial tumor volume for each mouse (left). Different colors/symbols represent individual mice. The recurrence incidence is summarized (right). **D.** CCR2 antagonist suppresses castration-induced regression in Hi-MYC prostate cancer-bearing mice. Red circles: mice were castrated and received vehicle. Blue boxes: mice were castrated and received CCR2i prior to castration. N=5 for each group. The recurrence incidence is summarized (right). Tumor volume kinetics for individual mice are in Figure 40.

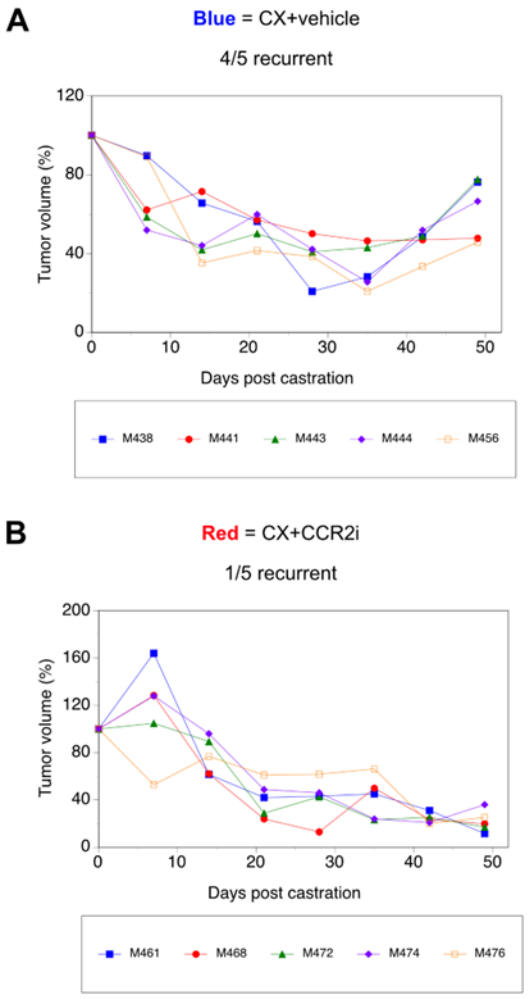

Figure 10. CCR2 inhibitor suppresses castration-induced regression in Hi-MYC prostate cancer-bearing mice: related to Figure 39D. Tumor volume kinetics for individual mice that are summarized/averaged in Figure 9D.

We used a transcriptomic approach to further investigate CCL2 signaling, immune cell migration, and TAMs in the development of castration-resistant prostate cancer in the PTEN-deficient GEMM. Differential gene expression (DGE) analysis was performed on bulk RNA-sequencing data from tumor tissue (Figure 11) and the resulting sets of genes with FDR<0.05 and |log2FC| were subjected to Gene Ontology (GO) enrichment analysis.

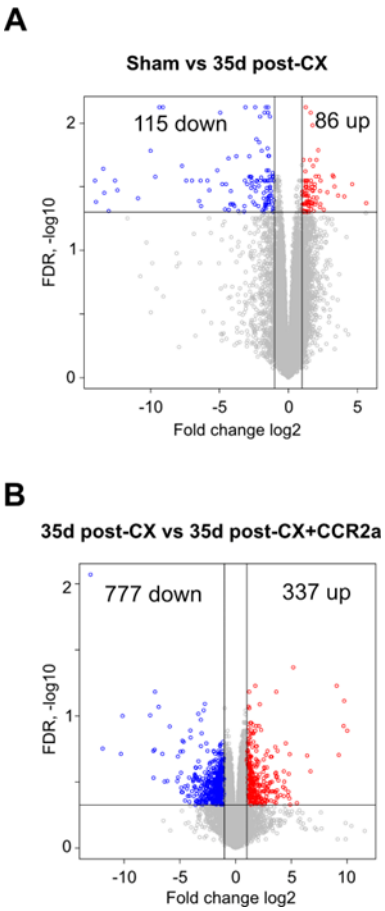

Figure 11. Volcano plots of differentially-expressed gene (DEG) analysis: related to Figure 12. RNA was extracted from PTEN-deficient tumors from the following mice: sham-operated (Sham), 35d post-castration (35d post-CX) and 35d post-castration after receiving CCR2a (35dp-CX+CCR2a). DEG was performed on bulk RNAseq data using RNAseq transcript sets derived from tumors in mice that were sham-operated vs mice 35d post-castration (**A**) or from tumors in mice 35d post-castration vs mice treated with CCR2a 35d post-castration (**B**).

These analyses revealed that a very similar category of gene sets – mediating immune cell chemotaxis and migration – are up-regulated in the bulk tumor mRNA from mice 35 days post-castration (vs. sham-operated mice; Figure 12A) but down-regulated in the bulk tumor mRNA from mice 35 days post-castration which were treated with CCR2a (Figure 12B). We also assembled a TAM-related gene set and found that these genes are similarly regulated: 'up' in the 35 days post-castration group and 'down' in the 35 days post-castrated group treated with CCR2a (Figure 12C).

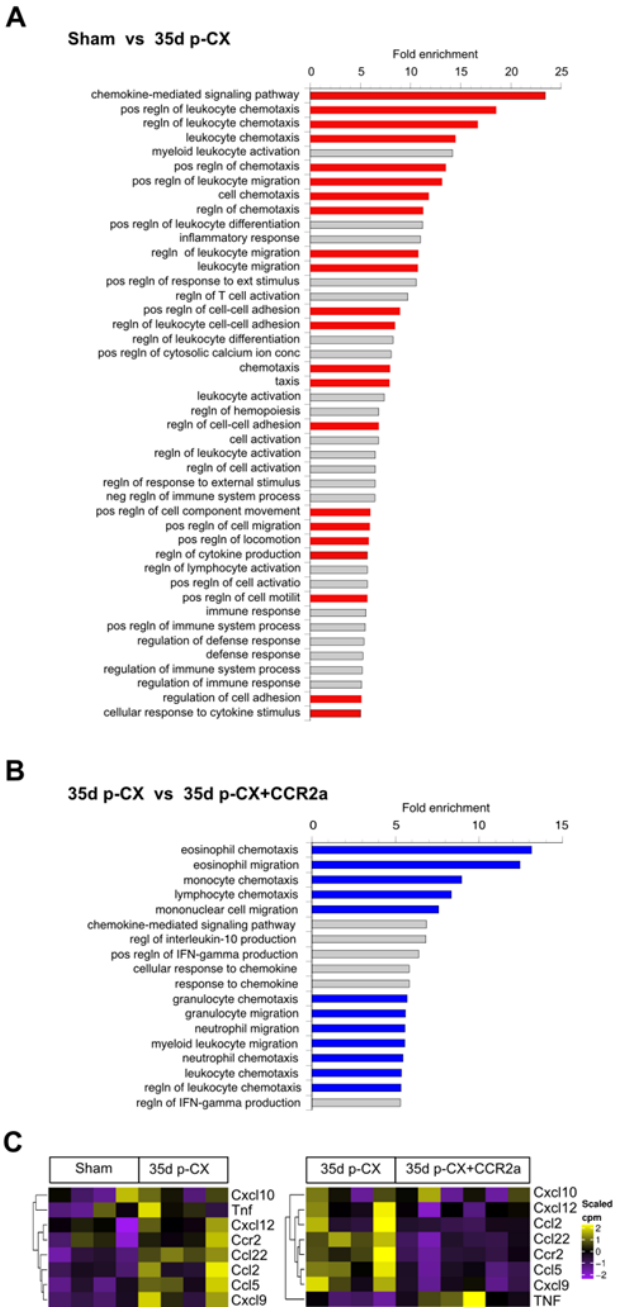

Figure 12. Transcriptomic changes in PTEN-deficient prostate cancers following CCL2 signaling blockade. RNA was extracted from PTEN-deficient tumors from the following mice: sham-operated (Sham), 35d post-castration (35d post-CX) and 35d post-castration after receiving CCR2a (35dp-CX+CCR2a). DGE analysis was performed on bulk RNAseq data (Figure 41) followed by Gene Ontology analysis of biological processes comparing RNAseq transcript sets derived from tumors in mice that were sham-operated vs mice 35d post-castration (**A**) or from tumors in mice 35d post-castration vs mice treated with CCR2a 35d post-castration (**B**). Red-colored bars represent up-regulation and blue-colored bars represent down-regulation. Fold-enrichment >5. **C.** TAM-related transcripts regulated by CCL2 signaling. Heatmap representation of mRNA levels of select TAM-associated genes for the same two comparisons shown in **A** (left) and **B** (right).

An immunosuppressive cell profile is induced in the TME during castration-resistant recurrence.

Taken together, the analyses in Figures 9 and 12 indicate that CCL2 might be functioning to recruit TAMs and drive the progression to, or recurrence as, castration resistant prostate cancer. Thus, to determine how TNF-CCL2 signaling effects the tumor immune microenvironment in the PTEN-deficient murine prostate cancer model, we used immunohistochemistry (IHC) to quantitate CD68- and CD8-stained cells in tissue sections from the tumors. As seen in Figure 13A, CD68-stained cells (presumptive TAMs) increase, most notable at 35 days post-castration, just as tumor re-growth in the recurrence phase is beginning. In addition, etanercept partially blocks this increase in TAMs and coordinately inhibits tumor recurrence. CD8 T cells (presumptive cytolytic T-lymphocytes; CTLs) decreased over time following castration and this was also partially reversed by etanercept administration to the mice bearing PTEN-deficient tumors. Figure 13B demonstrates that blocking CCL2 signaling with the CCR2 antagonist has the expected effect – it reduces CD68-stained cells and increased CD8-stained cells, reversing the castration-induced immunosuppressive cell profile and coordinately preventing prostate cancer recurrence (Figure 9C).

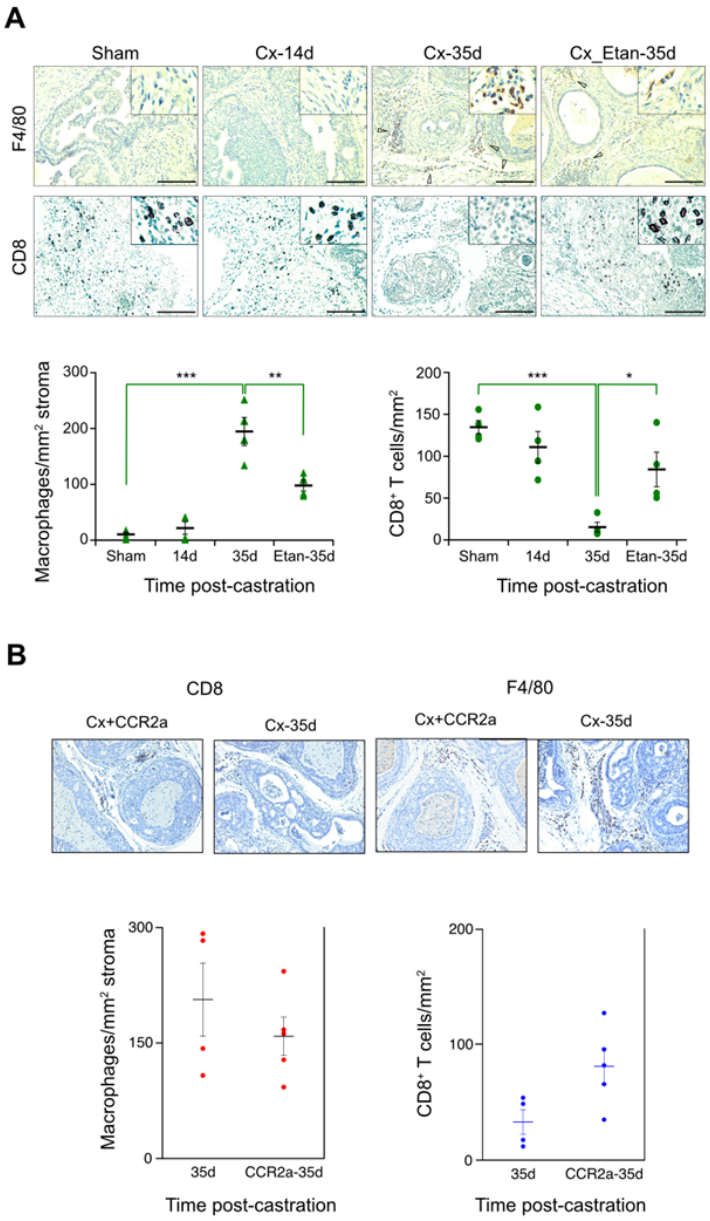

Figure 13. TNF and CCR2 signaling blockade suppress castration-induced immunosuppression at late times following castration. Mice bearing PTEN-deficient tumors were sham-operator or castrated (Cx) and tumors harvested at the indicated times post-castration. Some mice received etanercept (Etan) or the CCR antagonist BMS IHC staining for stromal F4/80+ macrophages and CD8+ T cells was performed and the number of stained cells per unit area were plotted. **A**. TNF signaling blockade. Images of representative IHC-stained tissue sections for the surface marker protein noted on the left side. Mice were treated as shown across top and the cell densities plotted for each of the treatments, below. **B**. CCL2 signaling blockade. Similar to **A** with both surface marker protein and treatments shown along the top. Staining and counting of the Cx-35d samples in **A** and **B** were performed separately. Data are given as mean ± s.e.m. (n=4). *p<0.05, **p<0.01, ***p<0.001 (One-way ANOVA followed by Tukey-Kramer HSD test).

4.4.6 Transcriptomic CD8 / CD68 ratio predicts castration outcome.

Next, we carried out transcriptomic profiling to confirm the IHC studies in Figure 13, which correlated an immunosuppressive immune cell profile (elevated CD68, reduced CD8) with recurrence of the PTEN-deficient tumor. Specifically, three mice bearing PTEN-deficient prostate cancers were castrated and tumor volume was HFUS-monitored for 42 days (Figure 14A). One mouse failed to regress and was labeled 'stable'. Two mice regressed, one of which showed recurrence 21 days after castration. We recovered the tumors, and performed single cell RNA sequencing. Transcript count data was pooled and tSNE dimensionality reduction was used to along with subjective cell annotation to identify 6 cell populations (Figure 14B). Among CD45-positive immune cells, TAMs were identified as those cells expressing both CD68 and CD80, while cytolytic T-cells (CTL) were defined as those expressing CD3 and CD8 (see details in the legend to Figure 44). In Figure 14C, we plotted the ratio of CTL to TAM, and observed that compared with the regressing tumor, the recurrent tumor had a lower CTL/TAM ratio. This is consistent with the IHC analysis in Figure 13A and suggests that immune suppression drives tumor re-growth.

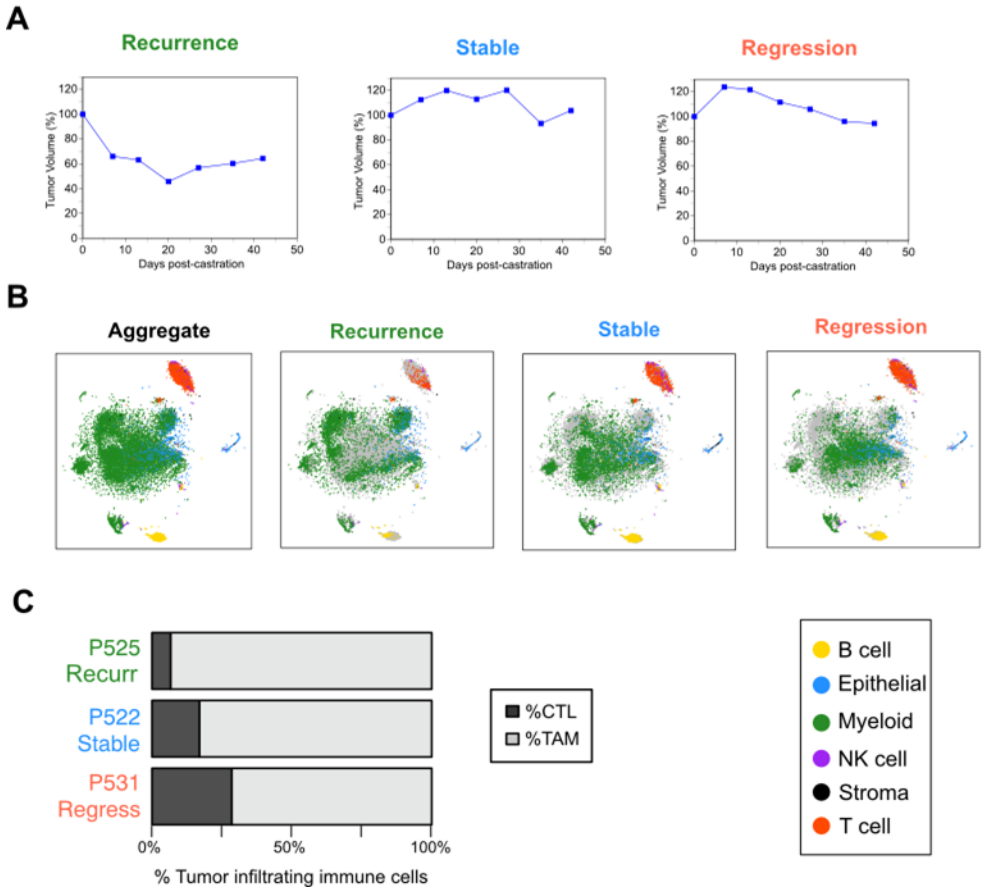

Figure 14. Tumor recurrence following castration correlates with an immunosuppressive tumor microenvironment. **A.** Tumor volume kinetics for three representative PTEN-deficient mouse tumors. Tumor volumes were determined by serial HFUS imaging and 3D reconstruction and plotted after normalizing to the initial tumor volume for each mouse. **B.** t-SNE plots for single cell RNAseq analysis. At 42d post-castration, mice were sacrificed, tumor tissue was disaggregated into single cell preparations, RNA sequenced and analyzed as described in the Methods. Dimensionality reduction was performed with tSNE. **C.** CTL:TAM ratios for regressing, stable or recurrent mouse tumors. Transcriptomic data from **B** was used to define TAMs ($CD45^+$ and $CD68^+$and $CD80^+$; lighter grey) and CTLs (CD45 and [CD3e or Cd3d or CD3g] and [CD8a or CD8b1]; darker grey). See text for discussion. We used a transcriptomic approach to further investigate CCL2 signaling, immune cell migration, and TAMs in the development of castration-resistant prostate cancer in the PTEN-deficient GEMM.

Accomplished under Aim 3

In Aim 3, we continue to collect and store samples for future batch-wise analysis. While participant accrual was affected by the covid-19 pandemic, we have resumed accruing participants at pre-2020 rates. We have enrolled 4 participants in Arm A (ADT only, target 10) and accrued biospecimens from 2 of these (the therapy paradigm has evolved precluding additional participants in accord with standard of care therapy, and this Arm will close upon completion of the study not fully enrolled). We have enrolled 21 participants in Arm B (ADT plus XRT, target 20) and accrued biospecimens from 18 of these, with 3 participants remaining on study (we expect to close this Arm in early 2023). We have enrolled 11 participants in Arm C (XRT only, target 20) and accrued biospecimens from 9 of these. Upon completion of biospecimen accrual, analysis will commence.

What opportunities for training and professional development has the project provided?
Nothing to report.

How were the results disseminated to communities of interest?
Nothing to report.

What do you plan to do during the next reporting period to accomplish the goals?

We will prepare a manuscript documenting our results from Aims 2. We plan on competing enrollment for the study of Aim 3, and undertake biospecimen analysis for TNF and CCL2.

4. IMPACT:

What was the impact on the development of the principal disciplines of the project?

We demonstrated that demonstrated that castration led to tumor regression in a PTEN-deficient mouse model, followed by the expansion of a basal stem-like cell population and TNF secretion, likely from this basal stem-like population. At the late (~5 week) time point, increased TNF secretion correlated with tumor recurrence and TNF-induced, NFkB-mediated CCL2 secretion. CCL2 production, in turn,

recruits TAMs, reduces CTLs and enhances tumor proliferation and recurrence. We observed that downregulation of TNF-induced NF-κB signaling at 6 days following castration. Inhibition of downstream anti-apoptotic genes indicated ADT induced regression was mediated by apoptosis. At 35 days after castration, TNF-induced NF-κB signaling was upregulated. Applying CCR2 antagonist one day prior to castration, the tumor volume phenocopied the tumor volume response seen with sTNFR2-Fc treatment. TNF mRNA expression from bulk RNA-seq analysis remained unchanged in CCR2-blockade castrated mice, further indicating that CCL2 is a downstream target of TNF. We observed that CCR2a treatment prior to castration was comparably effective at inhibiting castration-resistant recurrence in Hi-MYC mice, and resulted in similar changes seen in the PTEN-deficient model. Gene sets mediating both immune cell chemotaxis and migration and a TAM-related gene set were up-regulated in mice 35 days post-castration but down-regulated in mice 35 days post-castration which were treated with CCR2a. This suggests that CCL2 might be functioning to recruit TAMs and drive the progression to, or recurrence as, castration resistant prostate cancer. Indeed, CD68-stained cells (presumptive TAMs) increased and CD8 T cells (presumptive cytolytic T-lymphocytes; CTLs) decreased after castration, just as tumor re-growth in the recurrence phase is beginning. Etanercept and CCR2 antagonist partially blocks these changes and coordinately inhibits tumor recurrence. Finally, single-cell transcriptomic analysis determined that CD8 / CD68 ratio predicts castration outcome and suggests that immune suppression drives tumor re-growth.

What was the impact on other disciplines?
Nothing to report

What was the impact on technology transfer?
Nothing to report

What was the impact on society beyond science and technology?
Nothing to report

5. CHANGES/PROBLEMS:
Nothing to report

Changes in approach and reasons for change

Actual or anticipated problems or delays and actions or plans to resolve them
The post-doctoral fellow, Dr. Aerken, experienced immigration issues, and thus was unable to participate in the project research effort for the final three months of the period. The study statistician, Dr. Eng, left Roswell Park, and thus was unable to participate in the project research effort for the final six months of the period. The study PI, Dr. Krolewski, retired from Roswell Park at the end of the reporting period. These changes delayed progress, and Co-I Dr. Nastiuk was approved by the grants and program officers as PI of the award during a one year NCE period.

Changes that had a significant impact on expenditures

Personnel departures resulted in unanticipated funds remaining at the end of the initial performance period. A one year no-cost extension was approved by the grants and program officer to complete the proposed tasks.

Significant changes in use or care of human subjects, vertebrate animals, biohazards, and/or select agents
Nothing to report

6. PRODUCTS:

Publications.

Krolewski, JJ, Singh, S, Sha, K, Jaiswal, N, Turowski, S, Pan, C, Rich, L, Seshadri, M, Nastiuk, KL. (2022). TNF signaling is required for castration-induced vascular damage preceding prostate cancer regression. Cancers 14:6020.

Other publications, conference papers and presentations.

Nothing to report

Website(s) or other Internet site(s)

Nothing to report

Technologies or techniques

Nothing to report

Inventions, patent applications, and/or licenses

Nothing to report

Other Products

Nothing to report

7. PARTICIPANTS & OTHER COLLABORATING ORGANIZATIONS

What individuals worked on the project?

John Krolewski, MD PhD. PI. 2.4 Calendar Months.

- Dr. Krolewski lead the project and analysis of the data for manuscript #2.

Kent Nastiuk, PhD. Co-Investigator, 3.6 Calendar Months

- Dr. Nastiuk helped to supervise the post-doctoral fellow in the lab, managed the imaging experiments and assisted with the analysis of the data. He lead the writing of publication #1.

Kevin Eng, PhD. Biostatistician, 0.48 Calendar Months

- Dr. Eng assisted with statistical analysis of the regression and recurrence kinetics.

Aerken Maolake, PhD. Post-doc. 3 Calendar Months.

- Dr. Maolake carried out bench work on the project.

Jessica Herrington, BS. Post-Bac. 1 Calendar Months.

- Ms. Herrington banked biospecimens for the project.

Gurkamal Chatta, MD. Co-investigator. 0.24 Calendar Months

- Dr. Chatta assisted with Aim 3.

Bo Xu, MD, PhD. Co-investigator. 0.24 Calendar Months

- Dr. Xu assisted with Aim 3.

During the NCE year, Drs. Maolake, Jaiswal, Eng, Xu, Chatta, and Krolewski are no longer participating in the project. Ms. Zhang is no longer participating in the project.

Has there been a change in the active other support of the PD/PI(s) or senior/key personnel since the last reporting period?

Dr. Nastiuk has 0.9 Calendar months support from W81XWH-19-0397, entitled "Hereditary X-linked Tumor Suppressor Escapes Immune Control in Prostate Cancer" during the NCE year of this project. There is no overlap with this project.

Dr. Nastiuk has 1.2 Calendar months support from R01 CA260375-01, entitled "Applying pathomics to establish a biosignature for aggressive skin melanoma" during the NCE year of this project. There is no overlap with this project.

Dr. Nastiuk has 0.6 Calendar months support from R01 CA222382-01A1, entitled "Preoperative respiratory muscle training to prevent postoperative pulmonary complications in patients undergoing resection for lung cancer" during the NCE year of this project. There is no overlap with this project.

What other organizations were involved as partners?
None

8. SPECIAL REPORTING REQUIREMENTS

Nothing to report

9. APPENDICES:

Krolewski, JJ, Singh, S, Sha, K, Jaiswal, N, Turowski, S, Pan, C, Rich, L, Seshadri, M, Nastiuk, KL. (2022). TNF signaling is required for castration-induced vascular damage preceding prostate cancer regression. Cancers 14:6020.

cancers

IMPACT FACTOR 6.575

Indexed in: PubMed

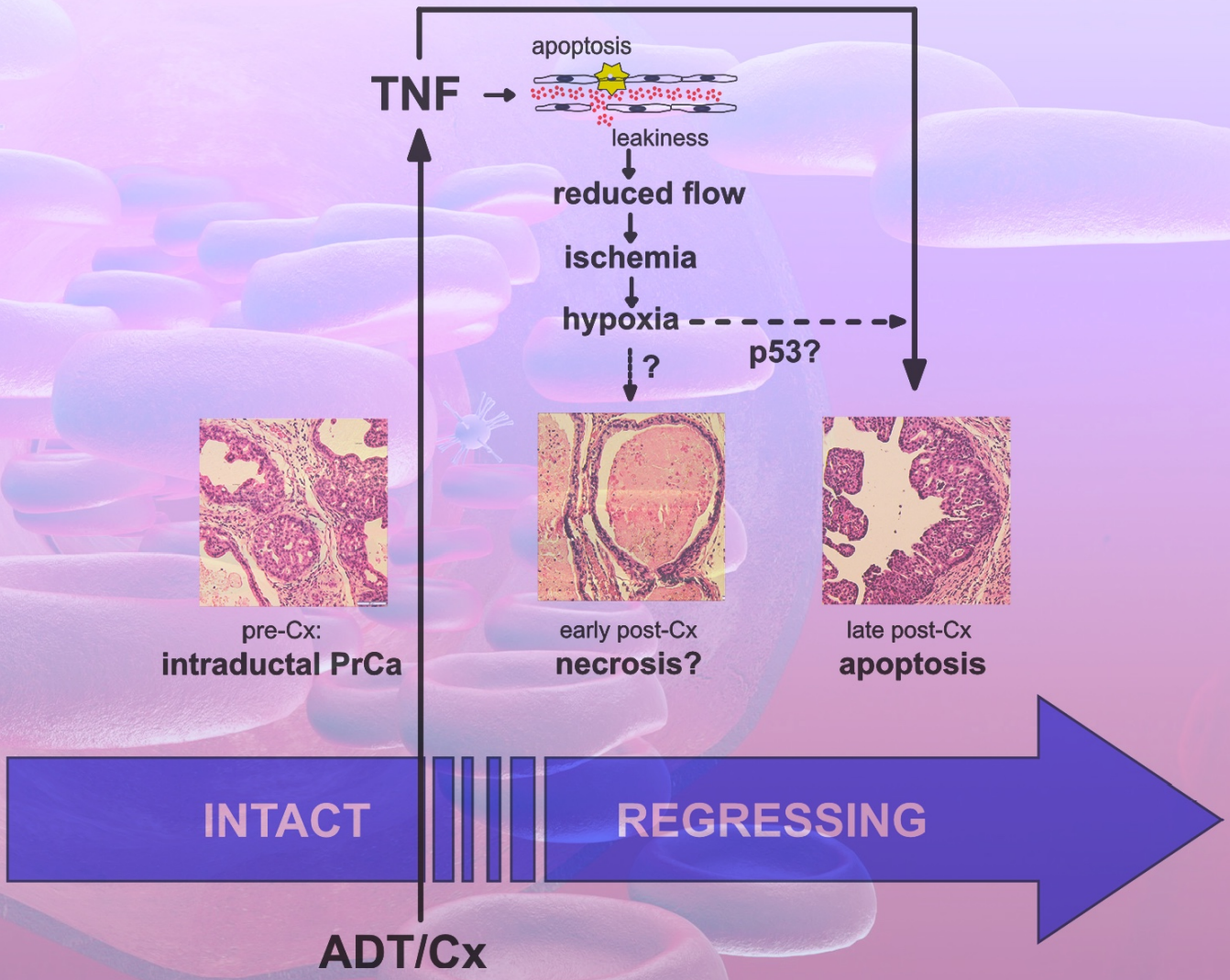

TNF Mediates Vascular Regression of Prostate Cancers

Volume 14 · Issue 24 | December (II) 2022

MDPI

mdpi.com/journal/cancers
ISSN 2072-6694

cancers

IMPACT FACTOR 6.575

Indexed in: PubMed

Article

TNF Signaling Is Required for Castration-Induced Vascular Damage Preceding Prostate Cancer Regression

John J. Krolewski, Shalini Singh, Kai Sha, Neha Jaiswal, Steven G. Turowski, Chunliu Pan, Laurie J. Rich, Mukund Seshadri and Kent L. Nastiuk

Special Issue

The Response of Prostate Cancers to Androgen Deprivation Therapies

Edited by

Dr. John J. Krolewski

MDPI

https://doi.org/10.3390/cancers14246020

cancers

MDPI

Article

TNF Signaling Is Required for Castration-Induced Vascular Damage Preceding Prostate Cancer Regression

John J. Krolewski [1,†], Shalini Singh [1], Kai Sha [1], Neha Jaiswal [1], Steven G. Turowski [2], Chunliu Pan [1], Laurie J. Rich [3], Mukund Seshadri [3] and Kent L. Nastiuk [1,4,*]

[1] Department of Cancer Genetics & Genomics, Roswell Park Comprehensive Cancer Center, Buffalo, NY 14263, USA
[2] Department of Cell Stress Biology, Roswell Park Comprehensive Cancer Center, Buffalo, NY 14263, USA
[3] Laboratory of Translational Imaging, Center for Oral Oncology, Roswell Park Comprehensive Cancer Center, Buffalo, NY 14263, USA
[4] Department of Urology, Roswell Park Comprehensive Cancer Center, Buffalo, NY 14263, USA
* Correspondence: kent.nastiuk@roswellpark.org; Tel.: +1-716-845-5771
† Current address: Buffalo State College, State University of New York, Buffalo, NY 14222, USA.

Simple Summary: Androgen deprivation therapy (ADT) is the principal therapy for advanced prostate cancer. ADT controls tumor growth by rapidly altering the prostate tumor microenvironment and subsequently inducing cancer cell death. ADT induces prostate vascular damage and thereby reduces intratumoral blood flow in the rodent and human prostate gland, but the mechanism whereby ADT induces vascular damage has long been elusive. This work describes studies that, for the first time, functionally define TNF as the mediator of castration-induced vascular damage in prostate tumors.

Abstract: The mainstay treatment for locally advanced, recurrent, or metastatic prostate cancer (PrCa) is androgen deprivation therapy (ADT). ADT causes prostate cancers to shrink in volume, or regress, by inducing epithelial tumor cell apoptosis. In normal, non-neoplastic murine prostate, androgen deprivation via castration induces prostate gland regression that is dependent on TNF signaling. In addition to this direct mechanism of action, castration has also been implicated in an indirect mechanism of prostate epithelial cell death, which has been described as vascular regression. The initiating event is endothelial cell apoptosis and/or increased vascular permeability. This subsequently leads to reduced blood flow and perfusion, and then hypoxia, which may enhance epithelial cell apoptosis. Castration-induced vascular regression has been observed in both normal and neoplastic prostates. We used photoacoustic, power Doppler, and contrast-enhanced ultrasound imaging, and CD31 immunohistochemical staining of the microvasculature to assess vascular integrity in the period immediately following castration, enabling us to test the role of TNF signaling in vascular regression. In two mouse models of androgen-responsive prostate cancer, TNF signaling blockade using a soluble TNFR2 ligand trap reversed the functional aspects of vascular regression as well as structural changes in the microvasculature, including reduced vessel wall thickness, cross-sectional area, and vessel perimeter length. These results demonstrate that TNF signaling is required for vascular regression, most likely by inducing endothelial cell apoptosis and increasing vessel permeability. Since TNF is also the critical death receptor ligand for prostate epithelial cells, we propose that TNF is a multi-purpose, comprehensive signal within the prostate cancer microenvironment that mediates prostate cancer regression following androgen deprivation.

Keywords: photoacoustic imaging; tumor hypoxia; contrast-enhanced ultrasound; tumor perfusion; power Doppler; tumor blood flow; endothelial; sTNFR2-Fc; cancer therapy; mouse models

Citation: Krolewski, J.J.; Singh, S.; Sha, K.; Jaiswal, N.; Turowski, S.G.; Pan, C.; Rich, L.J.; Seshadri, M.; Nastiuk, K.L. TNF Signaling Is Required for Castration-Induced Vascular Damage Preceding Prostate Cancer Regression. *Cancers* **2022**, *14*, 6020. https://doi.org/10.3390/cancers14246020

Received: 28 October 2022
Accepted: 2 December 2022
Published: 7 December 2022

1. Introduction

Prostate cancer (PrCa) is the second leading cause of cancer-related mortality in American men [1]. While localized PrCa can be cured in many men by surgery or radiation, androgen deprivation therapy (ADT) is the mainstay treatment for locally advanced, recurrent, or metastatic PrCa [2]. Prostate cancer regresses following ADT due to the death of epithelial-derived tumor cells [3]. Indeed, one of the earliest morphological descriptions of apoptotic cell death was in the luminal epithelial cells of the rat prostate gland following castration [4]. Tissue reconstitution experiments by Cunha and colleagues demonstrated that androgen blockade causes prostate cancer regression indirectly via stromal-derived soluble factors that act on the tumor epithelium [5]. For example, we previously demonstrated that stromal-derived tumor necrosis factor (TNF)—the prototypical death receptor ligand—mediates castration-induced regression in normal murine prostates [6]. Specifically, castration-induced regression of the normal prostate is reduced in both Tnfr1- and Tnf-deleted mice as well as mice treated with the TNF ligand trap drug etanercept [6].

Although castration-induced TNF signaling directly triggers epithelial cell apoptotic death in prostate cancers, there is substantial evidence that androgen withdrawal also affects the prostate tumor microvasculature [7,8]. Specifically, castration in rodent models leads to early induction of endothelial cell apoptosis and microvessel leakiness [9], a reduction in blood flow [10,11], and subsequent reduced perfusion of tumor tissue [12], which leads to ischemia and acute hypoxia [13–16]. A similar process of castration-induced microvasculature damage, caused by paracrine mediators, was observed in primary human xenografts [8]. Therefore, it has been proposed that there is a vascular phase or component to castration-induced regression of prostate cancers during which damage (apoptosis, leakiness) to the tumor microvasculature eventually produces tumor hypoxia. We suggest that the hypoxic state then either initiates or accelerates the necrotic and/or apoptotic death of epithelial tumor cells. The signaling mechanism that mediates ADT-induced vascular damage is unknown, but TNF has been shown to induce both endothelial cell apoptosis and vascular permeability [17,18] and is therefore a candidate for a secreted protein that can function in a paracrine manner to trigger vascular regression.

To test our hypothesis that TNF mediates the vascular component of ADT-induced regression, we monitored the effects of castration on the functional and structural properties of the tumor microvasculature in a c-Myc driven, androgen-sensitive prostate cancer model. We report that castration induced microvessel structural damage, reduced blood flow, reduced perfusion, and reduced oxygenation in the tumor, confirming and extending prior descriptions of vascular events accompanying regression in prostate cancer. Each of these functional and structural vascular alterations induced by castration were reversed by concurrent TNF signaling blockade, demonstrating that endogenous TNF signaling is necessary for castration-induced vascular regression and likely acts at the initiating step of the process, mediating endothelial cell apoptosis and vascular permeability. Combined with our previous studies, our findings suggest a comprehensive role for TNF signaling in ADT-induced regression of prostate cancer.

2. Materials and Methods

2.1. Cell Culture

The Myc-CaP cell line was established from the Hi-Myc transgenic mouse prostate [19], which were stably transfected with firefly luciferase under the androgen response element promoter [20]. Myc-CaP/ARE-luc cells were stored as low-passage aliquots, tested for mycoplasma and pathogens, and periodically renewed from frozen stock. Cells were grown in Dulbecco's Modified Eagle Medium containing glutamine and antibiotics with 10% fetal calf serum.

2.2. Animals

All animal studies were performed in accordance with the National Institute of Health Guidelines for the Care and Use of Laboratory Animals and approved by the Roswell

Park Institutional Animal Care and Use Committee (#1308M). Experimental studies were performed using two mouse models of PrCa, subcutaneous allografts of Myc-CaP cells, and an autochthonous, genetically engineered mouse model with prostate-specific Pten deletion [21]. All mice were maintained on a 12-h light and 12-h dark cycle and provided regular chow ad libitum.

To establish the Myc-CaP tumors, both flanks of male FVB/NCr mice (8–12 weeks old, Charles River Labs) were injected with 5×10^5 Myc-CaP/ARE-luc cells resuspended in equal volumes of RPMI media and Matrigel (Corning, Bedford, MA, USA). Tumor development was monitored by palpation and when evident, quantitated by high-frequency ultrasound (HFUS) imaging, as previously described [22]. Mice were treated and castrated or sham castrated 21 or 24 days after tumor cell injection. The average tumor volume at the time of castration was 382 ± 120 mm^3.

To produce prostate-specific PTEN loss-induced PrCa-bearing mice [21], male transgenic mice expressing probasin driven Cre recombinase (PB-cre4; obtained from NCI) were crossed with female floxed Pten mouse ($Pten^{LoxP/LoxP}$; obtained from JAX). The resulting pups were individually identified by implantation of a p-Chip (Pharmaseq, Monmouth Junction, NJ, USA) and genotyped for the Cre transgene and LoxP containing Pten alleles. At puberty, the probasin promoter is activated in prostate secretory epithelium, causing epithelial cell-specific deletion of Pten and thereby loss of PTEN activity. Prostate adenocarcinomas form with complete penetrance between 3 and 7 months. The animals were therefore monitored for tumor development using HFUS imaging beginning at 12 weeks. Tumor-bearing animals were enrolled for experimental manipulation when tumor size was between 300 mm^3 and 700 mm^3 (mean 436 ± 31 mm^3).

TNF signaling was blocked by treating mice with etanercept (Amgen, Thousand Oaks, CA, USA), using a regimen previously demonstrated to block castration-induced regression of the normal prostate gland [6]. Etanercept is the soluble extracellular portion of TNFR2 coupled to the IgG Fc domain (sTNFR2-Fc). At three days and one day prior to castration, tumor-bearing mice were treated with sTNFR2-Fc by intraperitoneal (ip) injection (4 mg/kg). Soluble TNF (PeproTech, Rocky Hill, NJ, USA) was injected (27 µg/kg) ip at the time of castration, at a dose sufficient to restore castration-induced prostate regression in TNF-deficient mice [6]. Control mice received PBS on the same schedule. Mice were surgically castrated on day zero, as previously described [23]. Briefly, animals were anesthetized using 2.5% isoflurane (Benson Medical Industries, Markham, ON, Canada) and maintained on 1% isoflurane in oxygen. Testes were removed via bilateral scrotal incision, the blood vessels and vas deferens were ligated, and scrotal incisions were closed by suturing (rather than stapling) to enable imaging of the peritoneum.

2.3. Anatomic and Functional Imaging

Ultrasound imaging with co-registered photoacoustic imaging (PAI) and power Doppler, contrast-enhanced ultrasound (CE-US), and B-mode high-resolution HFUS imaging were performed using a 256 element, 21 MHz linear-array transducer (LZ-250) with the Vevo LAZR system (VisualSonics Inc., Toronto, ON, Canada). After mice were anesthetized and depilated, B-mode ultrasound images were acquired from the peritoneum, and 3D reconstructions of the prostate tumors were computed using Amira 3D visualization software (v5.4.5, FEI Visualization Sciences Group) [22]. For power Doppler sonography, the parameters used for acquisition were: operating frequency, 16 MHz; pulse repetition frequency, 2 kHz; Doppler gain, 40; depth, 20.00 mm; width, 23.04 mm; clutter/wall filter, medium. To enable accurate comparison of the power Doppler data, the relative change in power Doppler signal was calculated for the 3D ROI covering the entire tumor. Multispectral PAI was performed to obtain measurements of oxygen saturation (sO_2). The PAI parameters used were: operating frequency, 21 MHz; depth, 23.00 mm; width, 23.04 mm; wavelength, 750/850 nm; total hemoglobin concentration threshold (Hbt), 20 arbitrary units; acquisition mode, sO_2/Hbt. The photoacoustic gain was kept at 43 dB and dynamic range at 20 dB for all studies. PAI-based measurements of oxygen saturation were calculated using the

two-wavelength approach (750/850 nm), as previously described [24,25], and the signal was measured for the 3D ROI covering the entire tumor. Nonlinear contrast mode imaging was performed to detect the presence of Vevo MicroMarker contrast agent (VisualSonics, Toronto, ON, Canada). The contrast agent consisted of phospholipid shell microbubbles filled with nitrogen and perfluorobutane (2.3–2.9 μm in diameter). A bolus injection of the contrast agent (1×10^8 microbubbles) was administered via tail vein injection using a 25-gauge needle. Images were acquired using the following parameters: operating frequency, 18 MHz; depth, 20.00 mm; width, 23.04 mm; with 35 dB contrast gain, gate size 6. Nonlinear detection of the contrast signal was performed in 3D by moving the transducer through the volume of the tumor at a step size of 0.152 mm. Multimodal imaging datasets were processed offline using VEVO CQ software (v1.4), utilizing manually drawn tumor regions with perfusion parameters derived from the intratumoral signal intensity time curves for the 3D ROI covering the entire tumor. All imaging datasets were analyzed using Vevo LAB (v.1.7.2) workstation software.

2.4. Immunohistochemistry

Mice were sacrificed 24 h after castration and tumors were collected for histology. Tumors were fixed in formalin-free immunohistochemistry zinc fixative (BD Pharmingen, San Diego, CA, USA) and 4 μm paraffin sections were obtained. Vessels were identified by immunohistochemical staining for CD31 (rat anti-mouse CD31, clone MEC13.3, #550274, BD Pharmingen) using an autostainer (Agilent/DAKO, Carpinteria, CA, USA), as previously reported [12]. Images were digitized using the ScanScope XT system (v12.4.6). The entire tumor area was delineated using Aperio ImageScope v11 software and vasculature integrity was analyzed using the default parameters of the automated microvessel analysis algorithm v1.1 (Aperio Technologies, Vista, CA, USA).

2.5. Statistical Analysis

Tumor volume and ELISA TNF protein levels were compared using one-way ANOVA and Dunnett's test post hoc. Saturated oxygenation, vascularity, and perfusion were analyzed using two-way ANOVA employing Tukey's honestly significant difference test post hoc to compare treatments over time. ANOVA two-tailed p-values < 0.05 were considered significant, and, if reached, post-hoc testing was performed. Unpaired Student's t-test was employed for single-treatment comparisons of histological parameters, and paired Student's t-test was used for single treatments analyzed using pre- and post-imaging. Two-tailed p-values < 0.05 were considered significant. All statistical analyses were performed using JMP Pro 11.0 software (SAS).

2.6. Data and Materials Availability

The data generated in this study are available within the article and its Supplementary Data files.

3. Results

To determine if TNF signaling plays a role in the vascular events accompanying castration-induced regression of prostate cancer, we employed a subcutaneously implantable Myc-CaP tumor model. The cell line used in this allograft model was derived from a prostate cancer that developed in Hi-MYC mice [19,26] that express the c-MYC oncogene in the prostate under the control of an androgen-regulated promoter (ARR_2/probasin-*Myc*). Since c-MYC amplification or overexpression is frequently observed in human prostate cancers [27], this model is relevant to human prostate cancers. We recently studied castration-induced vascular changes in Myc-CaP allografts implanted in mice as part of a study evaluating vascular targeting as a therapeutic strategy for treating prostate cancer [12]. In that report, we documented some of the vascular changes that have been previously described in castration-induced vascular regression [7]. In particular, one day following castration, we observed a reduction in tissue perfusion. Importantly, the effect

was similar in tumors implanted subcutaneously and orthotopically, allowing us to reliably use the subcutaneous model in the present study, since signals from some of the tissue imaging modalities we employ to assess vascular function are attenuated by tissue, making it difficult to make measurements on internal organs such as the prostate.

Myc-CaP tumors were implanted subcutaneously and tumor-bearing mice imaged by high-frequency ultrasound (HFUS) to monitor tumor size. Once tumors reached approximately 350–400 mm^3, mice were castrated and one day later (before there was a significant reduction in tumor volume, Supplementary Figure S1A), we measured changes in each step of the ordered sequence that defines the vascular contribution to tumor regression: (i) microvasculature damage; (ii) reduced blood flow; (iii) reduced tissue perfusion; and (iv) tissue hypoxia. To specifically test the role of TNF signaling, experiments were performed in the presence or absence of sTNFR2-Fc—a soluble form of the TNFR2 extracellular domain fused to the immunoglobulin Fc protein—that binds TNF and prevents signaling in the target cell.

3.1. TNF Is Necessary for Castration-Induced Microvasculature Damage in Myc-CaP Allografts

To test the role of TNF signaling in vessel structural changes, mice bearing Myc-CaP tumors were treated with vehicle or sTNFR2-Fc, followed by castration. Tumors were excised and formalin-fixed one day after castration, when active androgens were reduced at least 20-fold [28]. The microvasculature network was visualized using CD31 immuno-histochemical staining of tissue sections (Figure 1A) and then analyzed using an automated algorithm that determined microvessel density and related parameters. We previously reported that castration decreased the number of vessels in both subcutaneous and orthotopic Myc-CaP allografts by ~30% after one day [12]. sTNFR2-Fc treatment of castrated mice increased microvessel density in two of four tumors from mice (Figure 1B). In addition, the intratumoral area occupied by vessels, the vessel perimeter, and the thickness of the vessel walls were increased by sTNFR2-Fc treatment in all four tumors examined (Figure 1C–E). Taken together, these data were consistent with TNF mediating the vascular structural damage induced by castration in prostate tumors.

3.2. Castration-Induced Reduction in Blood Flow and Perfusion Is Prevented by Blocking TNF Signaling

Next, we used power Doppler imaging to quantitate the intensity of intratumoral blood flow. Doppler imaging uses high-frequency sound waves to visualize blood flow magnitude [29]. Power Doppler imaging has increased sensitivity versus color Doppler imaging, allowing more complete vessel function imaging by integrating speed and directional information [30,31]. Castration reduced the blood flow inside tumors (Figure 2A,B), but blood flow was not changed by castration when TNF signaling was blocked using sTNFR2-Fc (Figure 2C,D). While the castration-induced decrease in overall tumor blood flow was TNF-dependent one day after castration (Figure 2E, individual tumor changes at one day after castration are shown in Figure 2F), blood flow continued to decline with time. sTNFR2 treatment was not able to rescue the castration-induced reduction in blood flow four days after castration (Figure 2E). Serial measurement of changes in blood flow inside the same tumor confirmed the castration-induced reduction of blood flow was acutely TNF dependent (Figure 2G).

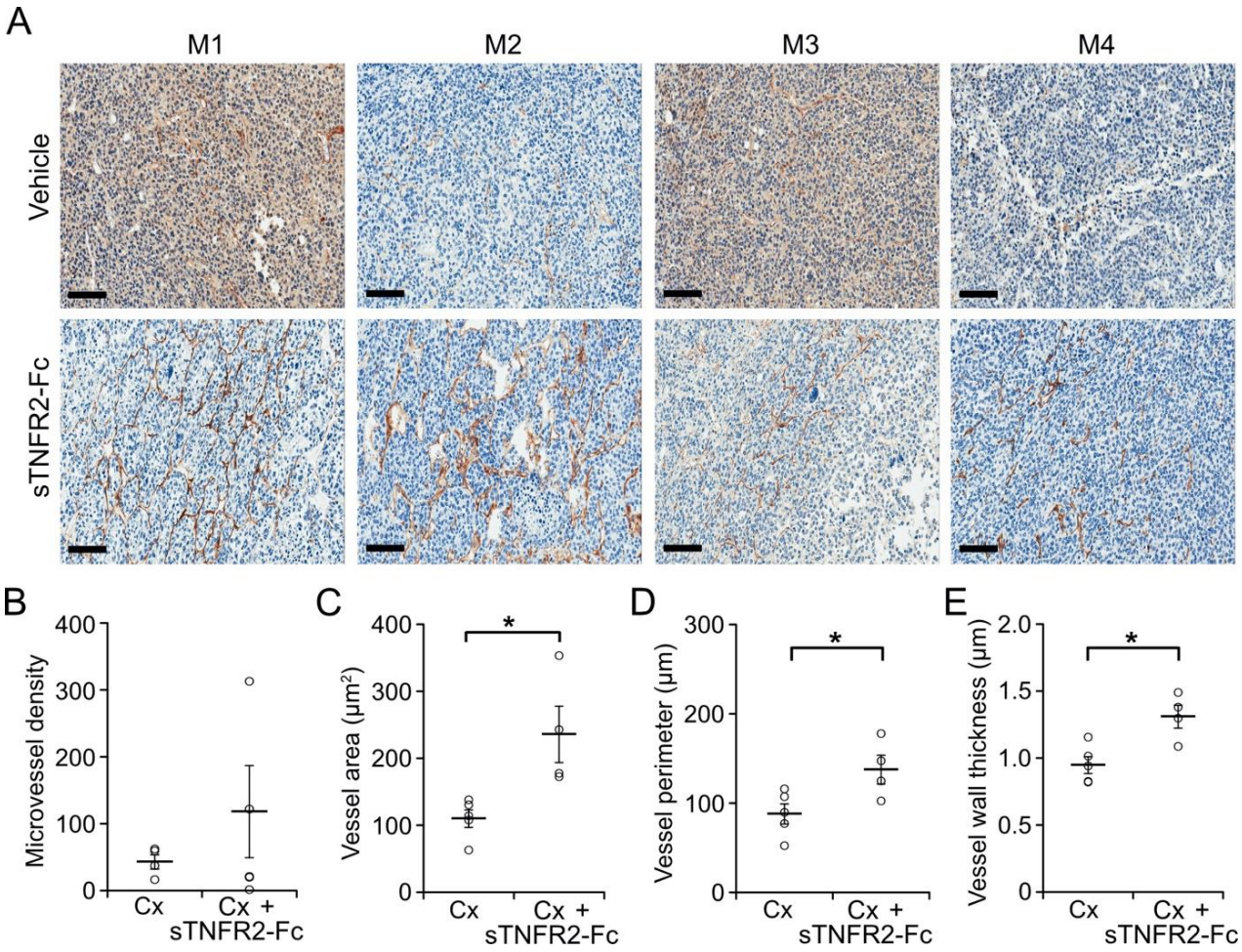

Figure 1. Castration-induced vascular damage is reversed by TNF signaling blockade. (**A**) Representative sections of CD31 immunoreactivity in Myc-CaP prostate tumors from four mice (M1–M4) castrated (upper panels) or castrated and treated with sTNFR2-Fc (lower panels). Scale bars are 100 μm. (**B**) Microvessel density (vessels per square millimeter). (**C**) Vessel cross-sectional area, in μm^2; (**D**) Vessel perimeter length, in μm; (**E**) Vessel wall thickness, in μm. (**B**–**E**) Large bars, means of measures from the tumors of five vehicle-treated castrated mice and from four sTNFR2-Fc-treated castrated mice (open circles), small bars = SEM. * $p < 0.05$.

To test if the changes in blood flow resulted in reduced tumor perfusion, Myc-CaP allografts were evaluated using contrast-enhanced ultrasound (CE-US) prior to and one day after castration of the host animal. Relative perfusion was determined using contrast agent accumulation in tumor capillaries and quantitated from a maximum intensity projection based on contrast accumulation. Figure 3 shows that castration reduced intratumoral perfusion (Figure 3A,B). However, castration did not reduce intratumoral perfusion in sTNFR2-Fc-pretreated host mice (Figure 3C,D). Tumors in sTNFR2-Fc-pretreated host mice were highly perfused, and this was also not changed by castration (Figure 3E). Castration-induced reduction of individual tumor perfusion was dependent on TNF signaling (blue versus red bars in Figure 3F, mean changes for all tumors shown in Figure 3G).

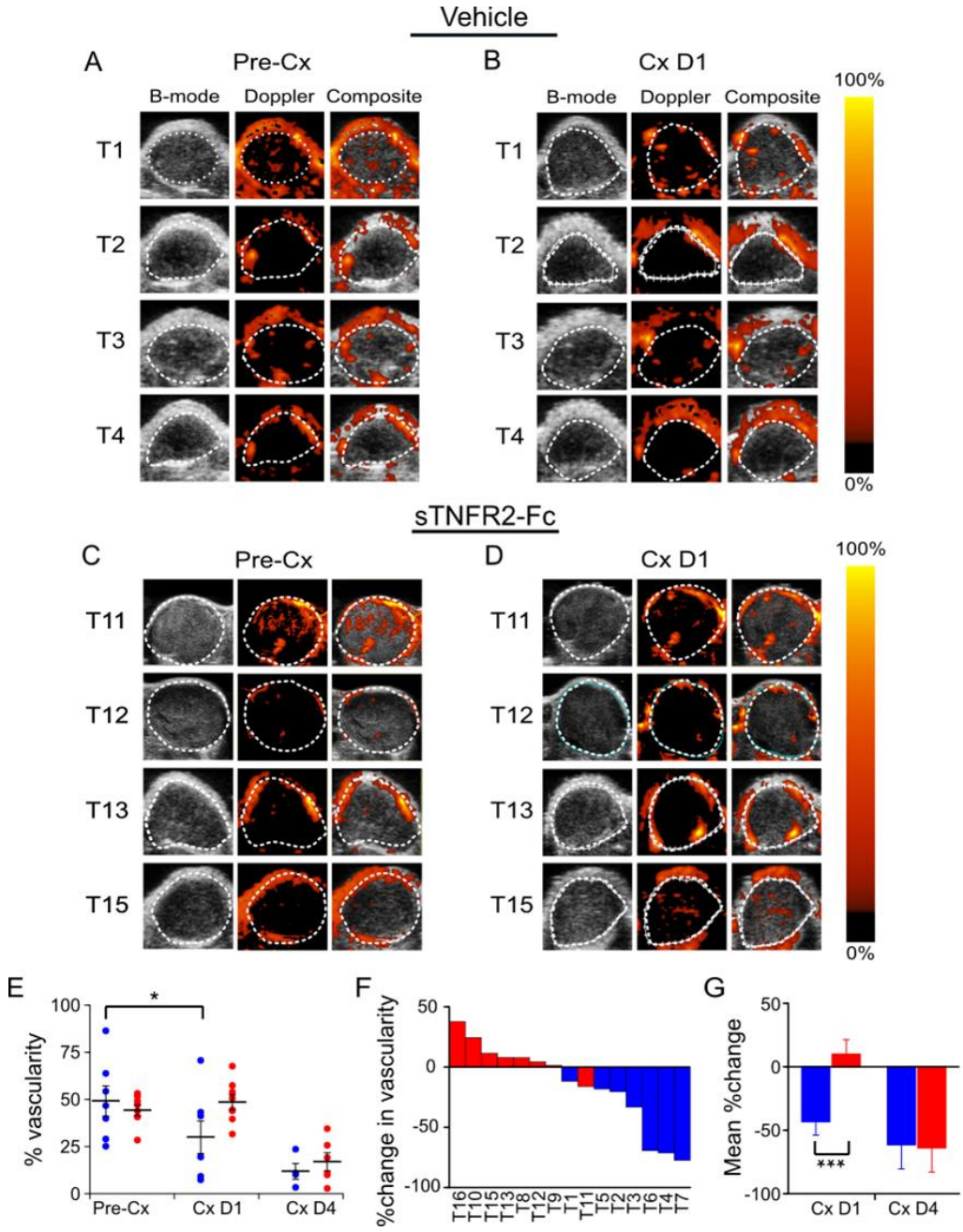

Figure 2. Castration-induced reduction of intratumoral blood flow in Myc-CaP tumor was dependent on TNF signaling. (**A**) Power Doppler (PD) images of subcutaneous Myc-CaP tumors pre-castration (Pre-Cx) of mice treated with PBS (Vehicle), tumors 1–4 (of 8 evaluable tumors). Left to right: Gray-scale ultrasound image (B-mode); PD pseudo-colored image to illustrate blood flow level (Doppler); Composite of PD image overlaid on the B-mode image (Composite). (**B**) PD images of tumors in panel A, one day after castration (Cx D1). (**C**) PD images of a second set of subcutaneous Myc-CaP tumors pre-castration of mice treated with sTNFR2-Fc, tumors 11, 12, 13, 15 (of 8 evaluable tumors). (**D**) PD images of tumors in panel C, one day after castration. (**E**) Mean PD signal (% vascularity, large bars) pre-castration, and at one and four days after castration from tumors in vehicle-treated (blue, D1 n = 8, D4 n = 7) and sTNFR2-Fc-treated mice (red, D1, D4 n = 8), PD signal of each tumor indicated by closed circles. (**F**) Waterfall plot of % change in vascularity in individual tumors at one day after castration. (**G**) Mean % change in paired measures of vascularity pre-castration versus D1 or D4 after castration. Columns and large bars are means and small bars are SEM. * $p < 0.05$, *** $p < 0.001$.

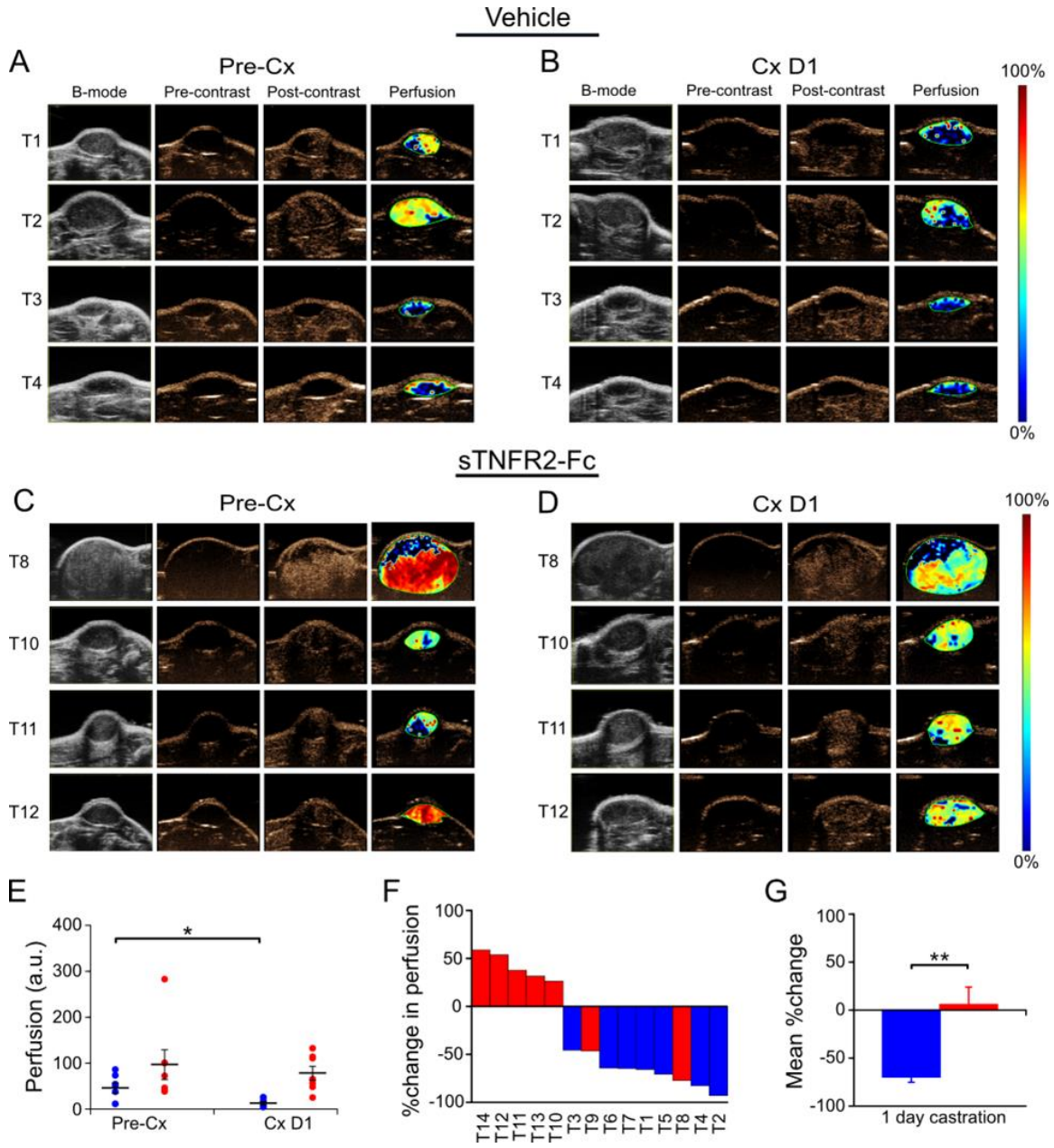

Figure 3. TNF signaling is necessary for castration-induced reduction of perfusion in Myc-CaP tumor. (**A**) Contrast-enhanced ultrasound (CE-US) images of subcutaneous Myc-CaP tumors pre-castration (Pre-Cx) of mice treated with PBS (Vehicle), tumors 1–4 (of 7 evaluable tumors) are shown. Left to right: Gray-scale ultrasound image (B-mode); contrast-mode image prior to contrast agent injection (Pre-contrast); contrast-mode image after injection at the peak enhancement of contrast (Post-contrast); pseudo-colored image of the change in contrast enhancement (Perfusion). (**B**) CE-US images of tumors 1–4 in panel A after one day castration (Cx D1). (**C**) CE-US images of a second set of subcutaneous Myc-CaP tumors pre-castration of mice treated with sTNFR2-Fc, tumors 8, 10, 11, 12 (of 7 evaluable tumors) are shown. (**D**) CE-US images of tumors in panel C, one day after castration, (**E**) Mean perfusion (large bars) pre-castration and post-castration in tumors in vehicle-treated (blue) and sTNFR2-Fc-treated (red) mice, perfusion signal of each tumor indicated by closed circles. (**F**) Waterfall plot of %change in perfusion in individual tumors (columns). (**G**) Average % change in perfusion pre-castration and post-castration. (**E**,**G**): Columns and large bars are means and small bars are SEM. * $p < 0.05$, ** $p < 0.01$.

3.3. TNF Is Required for Castration-Induced Hypoxia in Myc-CaP Allografts

Given our observations of reduced blood flow and perfusion, we next sought to determine the level of tissue oxygenation using photoacoustic imaging (PAI) to measure oxygen saturation. PAI can discriminate the absorption spectra of endogenous oxyhemoglobin from deoxyhemoglobin, enabling real-time 3D visualization of the microvasculature and measurement of changes in the percentage of hemoglobin oxygen saturation (%sO_2) [32]. As in prior experiments, Myc-CaP allograft volumes were measured using HFUS imaging and tumor-bearing mice were pretreated with sTNFR2-Fc (or vehicle) to block TNF signaling, and then castrated. One day after castration, the photoacoustic signal was decreased (Figure 4A) but no castration-induced change in photoacoustic signal was observed if TNF signaling was blocked using sTNFR2-Fc (Figure 4B). Castration induced a relative decrease in intratumoral hemoglobin oxygen saturation (%sO_2) one day after castration, but not when TNF signaling was blocked in host mice using sTNFR2-Fc (Figure 4C, individual tumor changes shown Figure 4D). The castration-induced hypoxia was not detectable four days after castration. Total intratumoral hemoglobin levels were not changed by either castration or sTNFR2-Fc treatment (Figure 4E). Grouped comparison of paired oxygenation changes in the same tumor revealed that castration-induced hypoxia was TNF dependent (Figure 4F).

3.4. TNF Is Required for Castration-Induced Hypoxia in an Autochthonous Prostate Cancer Model

To determine whether castration induces TNF-dependent vascular damage in a more clinically relevant prostate cancer model, we examined vascular change after castration in the endogenously arising PrCa tumors in PbCre4 $\times$ $Pten^{fl/fl}$ mice [21]. Tumorigenesis in this model is driven by Pten gene loss in the prostate epithelium. PTEN loss—similar to c-MYC gain of function—is one of the most frequent genetic lesions in both localized and metastatic human PrCa [33] and PTEN loss predicts outcome in patients [34]. Like human PrCa, these tumors grow slowly and regress within weeks after castration [21]. We first determined that TNF signaling did not acutely affect castration-induced regression (at one or four days) or acutely induce intratumoral TNF expression in this PrCa model (Supplemental Figure S2). Thus, these mice provide an excellent model to examine the role of TNF in acute ADT-induced vascular damage.

We tested if castration induced hypoxia in this model and whether the hypoxia was dependent on TNF signaling. Adult PbCre4 $\times$ $Pten^{fl/fl}$ mice (tumor volume 575 $\pm$ 32 mm^3) were pretreated with sTNFR2-Fc or vehicle, followed by castration. Tumor hypoxia levels were then assessed serially using PAI. Castration induced a decrease in the average %sO_2 in the tumors of vehicle-treated mice after one day (Figure 5A,C), but this effect was reduced after four days (Figure 5C). This castration-induced reduction in %sO_2 was abrogated in the tumors of mice pretreated with sTNFR2-Fc (Figure 5B,C). The observed PA signal (~4% sO_2) in this C57BL/6 PrCa model was much lower than in the Myc-CaP allografts (~20% sO_2) in white-colored hosts and in our previous report for a subcutaneous tumor model (~40% sO_2) in albino hosts [25], likely due to the black pigmentation artifact. Despite lower baseline %sO_2 levels, the paired change in %sO_2 (pre- versus post-treatment in the same tumor) was uniformly decreased in vehicle-treated mice at both one and four days after castration (blue, Figure 5D,E). This effect was blocked in most tumors of sTNFR2-Fc-pretreated mice after castration (red, Figure 5D,E). The castration-induced ~50% decrease %sO_2 (hypoxia) was reversed by sTNFr2-Fc pretreatment (Figure 5F). Power Doppler based measurements of blood flow and CE-US measurement of tumor perfusion were unchanged one or four days after castration in this PbCre4 $\times$ $Pten^{fl/fl}$ PrCa model (Supplementary Figure S3, and data not shown).

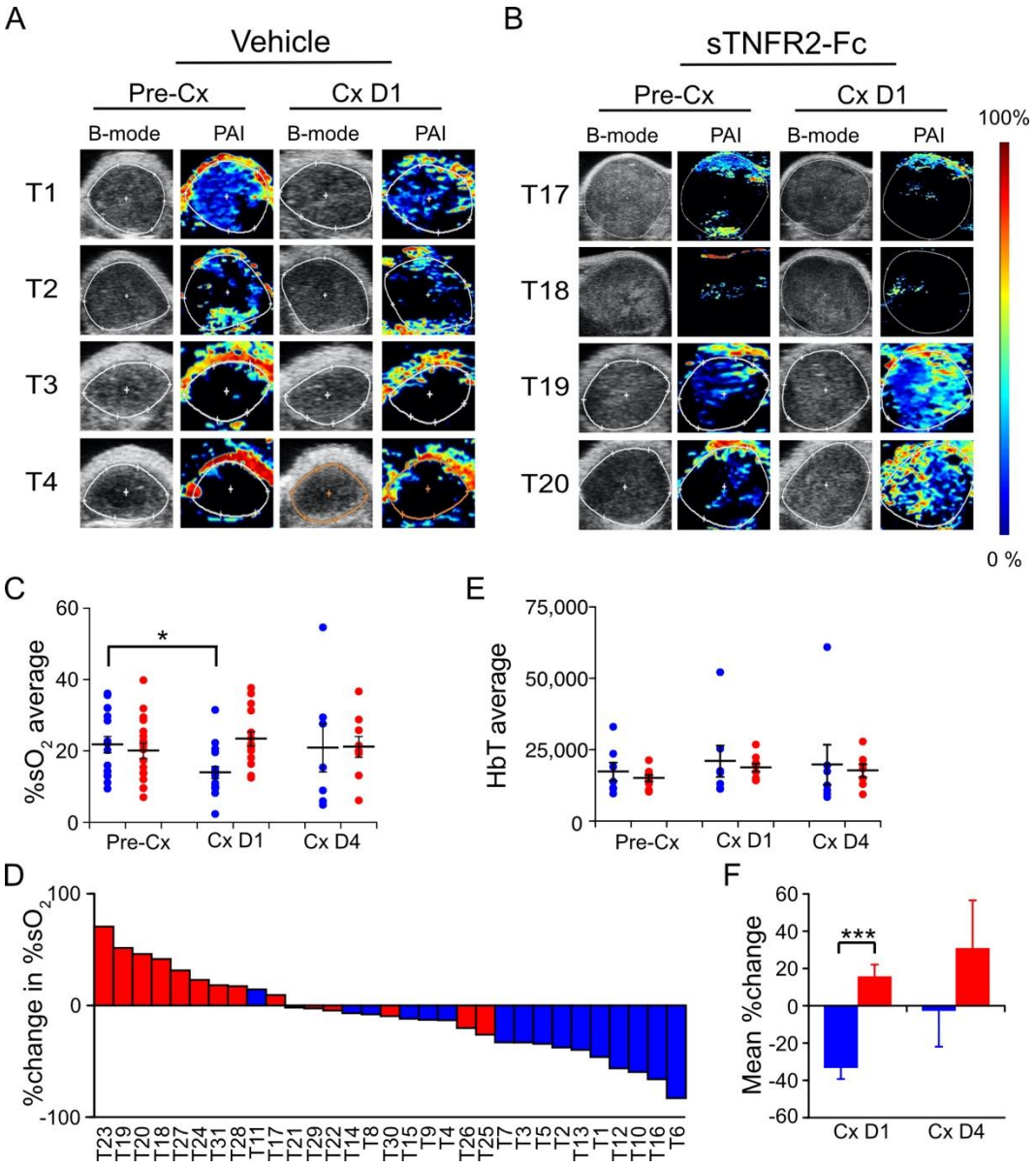

Figure 4. Castration-induced hypoxia in Myc-CaP tumor is reversed by TNF signaling blockade. (**A**,**B**) Photoacoustic images (PAI, pseudo-colored) and ultrasound (B-mode) of Myc-CaP subcutaneous tumors in four tumors from each group, pre- and post-castration from vehicle-treated mice (**A**) or sTNFR2-Fc-treated mice (**B**). (**C**) Mean PAI signal (%sO_2, large bars) from tumors pre-castration (n = 16), and at one (n = 15) and four (n = 9) days post-castration in vehicle-treated (blue) or in sTNFR2-Fc-treated (red) mice. PAI signal from each tumor indicated by closed circles. (**D**) Waterfall plot of change in %sO_2 in individual tumors at one day post-castration versus pre-Cx (columns). (**E**) Mean total hemoglobin (large bars) from tumors pre-castration (n = 16), and at one (n = 16), and at four (n = 14) days post-castration in vehicle-treated (blue) or sTNFR2-Fc-treated (red) mice. PAI signal of each tumor indicated by closed circles. (**F**) Mean change in paired measures of %sO_2 pre-castration versus D1 or D4 post-castration. Mean (columns) and SEM (bars). * $p < 0.05$, *** $p < 0.001$.

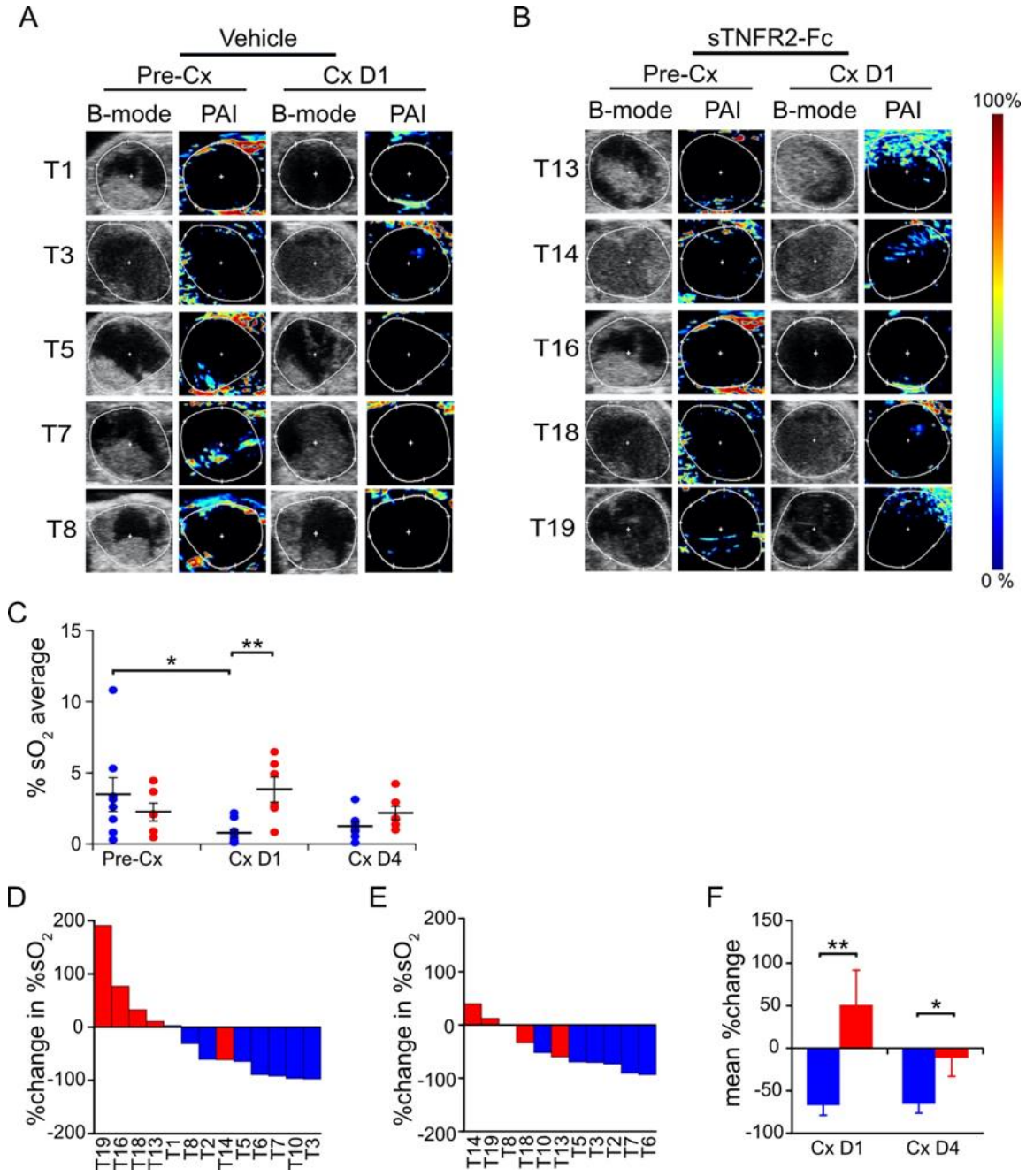

Figure 5. Castration-induced hypoxia is reversed by TNF blockade in prostate tumors of PbCre4 × Ptenfl/fl mice. (**A**,**B**) Photoacoustic images (PAI, pseudo-colored) and ultrasound (B-mode) of five tumors pre- and one day post-castration from vehicle-treated mice (**A**), or sTNFR2-Fc-treated mice (**B**). (**C**) Intra-tumoral mean PAI intensity (%sO_2 Average) pre-castration, and at one and at four days post-castration in vehicle-treated (n = 8, 8, 7 respectively, blue) or in sTNFR2-Fc-treated (n = 6, 5, 4 respectively, red) mice. (**D**) Waterfall plot of change in intra-tumoral %sO_2 one day after castration in mice treated with sTNFR2-Fc (red) or vehicle (blue). (**E**) Waterfall plot of change in intra-tumoral %sO_2 four days after castration in mice treated with sTNFR2-Fc (red) or vehicle (blue). (**F**) Change in paired measures of intra-tumoral %sO_2 pre-castration versus D1 or D4 after castration. Mean (columns or lines) and SEM (bars). * $p < 0.05$, ** $p < 0.01$.

3.5. TNF Is Necessary but Not Sufficient for Castration-Induced Hypoxia in Myc-CaP Allografts

Finally, since blocking TNF signaling was sufficient to abrogate castration-induced hypoxia, we tested whether soluble TNF was sufficient to induce hypoxia in Myc-CaP tumors.

When the Myc-CaP allografts became palpable, tumor volume was measured, PAI was performed, and then host mice were treated with TNF. TNF was administered at a dose sufficient to rescue TNF-mediated prostate regression in TNF-deficient mice [6]. Surprisingly, tumor oxygenation increased one day after TNF injection (Figure 6A). The TNF injection-induced change of $\%sO_2$ in individual tumors ranged from −20% to 240% (Figure 6B). Moreover, TNF protein levels were unchanged in soluble lysates of whole tumors after castration (Supplementary Figure S1B). These data suggested that in the subcutaneous Myc-CaP model, TNF signaling is necessary, but not sufficient, to trigger castration-induced intratumoral hypoxia. Instead, castration-induced modulation of downstream signaling in vascular cells must be required.

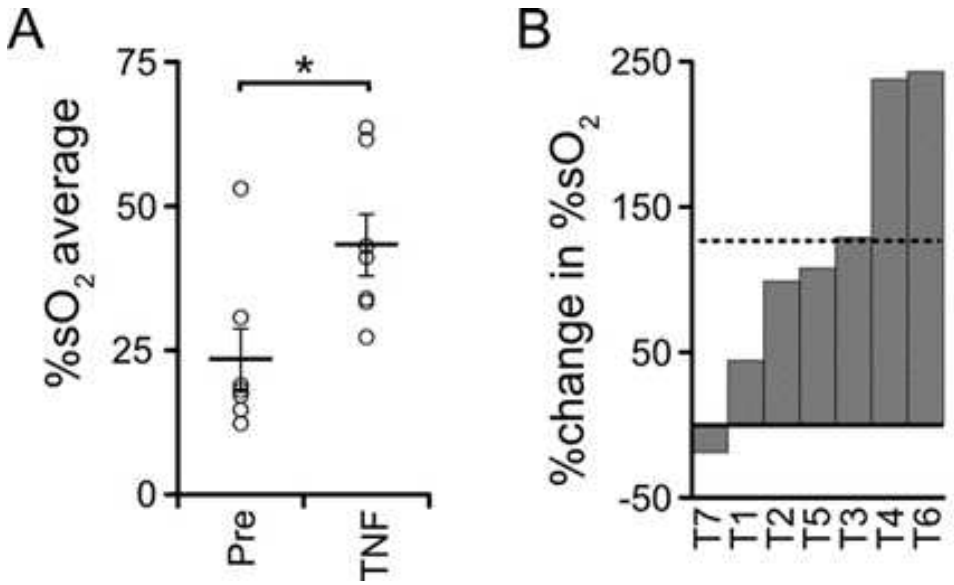

Figure 6. TNF in the absence of castration is insufficient to induce intra-tumoral hypoxia in Myc-CaP tumors. (**A**) Large bars, mean PAI signal ($\%sO_2$) from tumors pre-castration (n = 7), and at one day following TNF treatment (n = 7). PAI signals from individual tumors (open circles) and SEM (small bars). * $p < 0.05$. (**B**) Waterfall plot of %change in $\%sO_2$ in individual tumors (columns) after TNF treatment. Mean %change is dashed line.

4. Discussion

Previously, we reported that TNF (the prototypical death receptor ligand), but not other death receptor ligands such as FasL or TRAIL, was required for castration-induced regression of the normal murine prostate [6]. This is consistent with the original description of prostate cell death via apoptosis by Kerr et al. [4]. Treatment of normal mice with sTNFR2-Fc did not completely block castration-induced regression, suggesting that other apoptotic mechanisms are required for complete regression of the normal gland [6]. In this report, we employed complementary functional imaging modalities and vessel structural analysis to confirm and extend previous descriptions of the vascular component of regression. This pathological response to androgen deprivation—beginning with endothelial cell apoptosis and increased vessel permeability and culminating in hypoxia [13–16]—indirectly contributes to prostate cancer regression. In addition to a comprehensive analysis of vascular changes in the subcutaneous Myc-CaP model, we also detected castration-induced hypoxia in a genetically engineered PTEN-deficient prostate cancer model (Figure 5). We were not able to detect reduced blood flow by Power Doppler or reduced perfusion by CE-US in the PTEN-deficient model, perhaps because of limitations in imaging signal penetration for the endogenous prostate relative to the subcutaneous tumors (Figures 2–4).

We demonstrated microvessel damage using anti-CD31 immunohistochemistry, reduced blood flow via PD, reduced perfusion via CE-US, and hypoxia via PAI, all of which

were inhibited by blocking TNF signaling with sTNFR2-Fc. In agreement with previous reports [8,12,35,36], we found mixed changes in overall intratumoral microvessel density of sTNFR2-Fc-treated host animals after castration; however, we demonstrate TNF is necessary for castration-induced structural vessel damage, including diameter, area, and vessel wall thickness (Figure 1). These events all occur at one day post-castration, prior to the onset of tumor shrinkage (Supplementary Figures S1A and S2A). We have also recently observed that tumor volume in the PTEN-deficient model does not decrease until at least seven days following castration [28]. Despite this delay in tumor regression, intratumoral testosterone and dihydrotestosterone are reduced to near zero within 16 h of castration [28]. It has been shown that apoptosis rates in the endothelium increase prior to those in the epithelium [9], suggesting that endothelial damage occurs earliest. In addition, since we believe that the vascular events in Figures 1–4 are sequentially ordered (Figure 7), and since all are inhibited by sTNFR2-Fc, we conclude that TNF acts at the most proximal step. Indeed, there are multiple reports that TNF can induce both endothelial apoptosis and increase vascular permeability [17,18,37,38].

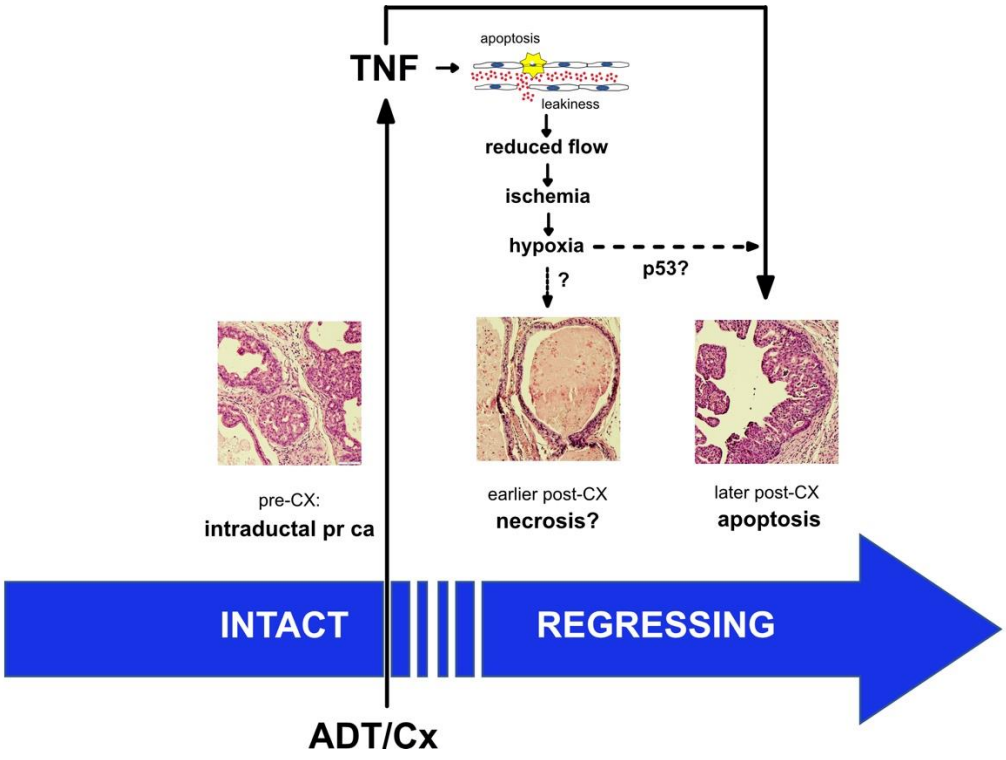

Figure 7. Proposed mechanism for TNF regulation of prostate regression. A proposed mechanism for prostate cancer regression following androgen deprivation therapy is illustrated, focusing on the contribution of events that are mediated by the tumor microvasculature. We propose that one of the earliest events is the activation of TNF signaling in endothelial cells, leading to increased permeability ('leakiness') and endothelial cell death. The damage to the endothelium leads to a cascade of vascular changes—reduced blood flow, ischemia due to reduced perfusion, and eventually transient tissue hypoxia—that likely enhances the death of the epithelial component of the tumor. A prediction of the model is that endothelial cell apoptosis precedes epithelial cell apoptosis, which has been noted in the literature (see text). There is limited support for the usual cell death consequence of hypoxia (namely necrosis or necroptosis), but there is a partial requirement for p53 in castration-induced regression, suggesting that p53-hypoxia signaling contributes to death receptor-mediated apoptosis of epithelial tumor cells.

Given that TNF signaling is the likely initiating signal for vascular regression, a key question is: what is the molecular trigger that activates TNF signaling in the endothelium?

In the normal prostate, we observed an acute increase in levels of TNF mRNA in the stromal compartment approximately 8 h post-castration [6]. In addition, we and others previously showed that c-FLIP is downregulated by castration via the androgen receptor acting on the c-FLIP promoter [39,40]. c-FLIP is a dominant-negative homologue of caspase-8 that acts as a natural inhibitor of death receptor signaling and its sustained expression may play a role in the development of castration-resistant prostate cancer [41]. In the models investigated in this report, TNF levels do not change acutely post-castration (Supplementary Figures S1A and S2A), suggesting that some other component of the TNF signaling cascade is regulated. Since the androgen receptor is only expressed in rodent pericytes, not endothelial cells [42], and pericyte AR regulates perfusion in other organs [43], prostate pericytes may be a key target for androgen regulation of TNF sensitivity via c-FLIP. Other components of the TNF apoptotic signaling network remain potential candidates for activating TNF signaling in the endothelium post-castration.

Our results also suggest a second key question: how does hypoxia lead to epithelial cancer cell death? One obvious result of tissue hypoxia is necrosis (or perhaps necroptosis). We detected necrosis in some tissue sections from the PTEN-deficient prostate cancer model (Figure 7), but we have not been able to document this on a consistent basis, nor did we observe necrosis in the Myc-CaP model. PTEN-deficient prostate cancers have an intraductal histology, which is observed in only a small fraction of human prostate cancers. Given the multiple layers of cancerous cells lining the ducts in these tumors, PTEN-deficient prostate cancers may be predisposed to hypoxia-induced necrosis. A more likely mechanism, especially in histologically typical prostate cancers, is that hypoxia activates or enhances epithelial apoptosis. Most primary prostate cancers express wild-type functional p53 (Supplementary Figure S4). Hypoxia induces p53 [44], which may then induce apoptosis during prostate cancer regression. Moreover, castration of p53 null mice yields partial regression of the normal prostate [45,46], implying a role for wild-type p53 in castration-induced regression. In the case of DNA damage stress, elevated p53 protein levels are known to induce cell cycle arrest and apoptosis via caspase-9 and Bcl-2 family proteins. However, hypoxia-induced p53 seems to function in a distinct fashion [47], with p53 transcriptionally regulating a distinct set of genes that encode apoptosis regulators [48]. Therefore, p53 induction could be a key molecular signal for hypoxia-induced epithelial apoptosis (Figure 7). Our hypothesis also suggests that patients with mutant p53 prostate cancers will not respond as well to ADT.

Finally, the TNF-mediated vascular damage caused by ADT may provide an opportunity for prostate cancer therapy. TNF administration induces short-duration vascular disruption in many cancers, transiently enhancing tumor permeability and ultimately reducing blood flow [49–51]. TNF therapy induces tumor regression in rodent models [52], but in humans it results in hypotension and other dose-limiting toxicities, thus preventing its effective use as a systemic anti-cancer therapy [53]. Neovasculature-targeted TNF circumvents this toxicity by producing locally high TNF levels and inducing vessel permeability [54], which enhances chemotherapy [55]. Similarly, tumor microenvironment-targeted TNF enhances CD8+ T-cell mediated anti-tumor immunotherapy [56]. We found that ADT, by inducing paracrine TNF signaling, disrupts the tumor vasculature in prostate tumors. However, the ADT-induced vascular damage is not durable, and tumor vascularization increased four weeks after castration [13]. A similar transient effect is observed in human tumors [8]. This suggests that ADT creates a window of vulnerability during which concurrently administered therapies may reduce cancer progression.

5. Conclusions

These results demonstrate that TNF signaling is required for vascular regression, most likely by inducing pericyte apoptosis and increasing vessel permeability. Since TNF is also the critical death receptor ligand for prostate epithelial cells, we propose that TNF is a multi-purpose, comprehensive signal within the prostate cancer microenvironment that mediated prostate cancer regression following androgen deprivation.

Supplementary Materials: The following supporting information can be downloaded at: https://www.mdpi.com/article/10.3390/cancers14246020/s1. Supplementary Figure S1: Tumor volume and TNF protein levels were not changed post-castration in prostate cancer allografts; Supplemental Figure S2: Tumor volume and TNF protein levels are not changed post-castration in autochthonous prostate cancers; Supplementary Figure S3: Castration does not alter blood flow in prostate tumors of PbCre4 × Ptenfl/fl mice; Supplementary Figure S4: TP53 mutation frequency in primary prostate cancers.

Author Contributions: Conception and design: M.S., J.J.K. and K.L.N.; Development of methodology: S.S., L.J.R., S.G.T. and K.L.N.; Acquisition of data: S.S., K.S. and C.P.; Analysis and interpretation of data: S.S., K.S., C.P., N.J., L.J.R., J.J.K. and K.L.N.; Writing, review, and/or revision of the manuscript: J.J.K., M.S. and K.L.N.; Study supervision: K.L.N. All authors have read and agreed to the published version of the manuscript.

Funding: This work was supported by the S.A.S. Foundation (grant no. HHS-6-15SF and HHS-009-17SF to K.L.N.), the ACS (grant no. 126771-IRG-14-194-11 to K.L.N.), the Roswell Park Alliance Foundation (K.L.N.), the Department of Defense Prostate Cancer Research Program (No. W81XWH-19-1-0378 to J.J.K.), and institutional support from the National Institutes of Health (No. S10OD010393-01, P30CA016056). The funders had no role in study design, data collection and analysis, decision to publish, or preparation of the manuscript.

Institutional Review Board Statement: All animal studies were performed in accordance with the National Institute of Health Guidelines for the Care and Use of Laboratory Animals and approved by the Roswell Park Institutional Animal Care and Use Committee (#1308M).

Data Availability Statement: Data generated or analyzed during the study are available from the corresponding author on request.

Acknowledgments: We thank the staff members of the Roswell Park Comprehensive Cancer Center's Experimental Tumor Models, Translational Imaging, and Laboratory Animal Shared Resources for their assistance.

Conflicts of Interest: The authors declare that there are no conflict of interest.

References

1. Siegel, R.L.; Miller, K.D.; Jemal, A. Cancer statistics, 2019. *CA Cancer J. Clin.* **2019**, *69*, 7–34. [CrossRef] [PubMed]
2. Sharifi, N.; Gulley, J.L.; Dahut, W.L. Androgen deprivation therapy for prostate cancer. *JAMA* **2005**, *294*, 238–244. [CrossRef] [PubMed]
3. Denmeade, S.R.; Lin, X.S.; Isaacs, J.T. Role of programmed (apoptotic) cell death during the progression and therapy for prostate cancer. *Prostate* **1996**, *28*, 251–265. [CrossRef]
4. Kerr, J.F.; Wyllie, A.H.; Currie, A.R. Apoptosis: A basic biological phenomenon with wide-ranging implications in tissue kinetics. *Br. J. Cancer* **1972**, *26*, 239–257. [CrossRef]
5. Kurita, T.; Wang, Y.Z.; Donjacour, A.A.; Zhao, C.; Lydon, J.P.; O'Malley, B.W.; Isaacs, J.T.; Dahiya, R.; Cunha, G.R. Paracrine regulation of apoptosis by steroid hormones in the male and female reproductive system. *Cell Death Differ.* **2001**, *8*, 192–200. [CrossRef]
6. Davis, J.S.; Nastiuk, K.L.; Krolewski, J.J. TNF is necessary for castration-induced prostate regression, whereas TRAIL and FasL are dispensable. *Mol. Endocrinol.* **2011**, *25*, 611–620. [CrossRef]
7. Buttyan, R.; Ghafar, M.A.; Shabsigh, A. The effects of androgen deprivation on the prostate gland: Cell death mediated by vascular regression. *Curr. Opin. Urol.* **2000**, *10*, 415–420. [CrossRef]
8. Godoy, A.; Montecinos, V.P.; Gray, D.R.; Sotomayor, P.; Yau, J.M.; Vethanayagam, R.R.; Singh, S.; Mohler, J.L.; Smith, G.J. Androgen deprivation induces rapid involution and recovery of human prostate vasculature. *Am. J. Physiol. Endocrinol. Metab.* **2011**, *300*, E263–E275. [CrossRef]
9. Shabisgh, A.; Tanji, N.; D'Agati, V.; Burchardt, M.; Rubin, M.; Goluboff, E.T.; Heitjan, D.; Kiss, A.; Buttyan, R. Early effects of castration on the vascular system of the rat ventral prostate gland. *Endocrinology* **1999**, *140*, 1920–1926. [CrossRef]
10. Shabsigh, A.; Chang, D.T.; Heitjan, D.F.; Kiss, A.; Olsson, C.A.; Puchner, P.J.; Buttyan, R. Rapid reduction in blood flow to the rat ventral prostate gland after castration: Preliminary evidence that androgens influence prostate size by regulating blood flow to the prostate gland and prostatic endothelial cell survival. *Prostate* **1998**, *36*, 201–206. [CrossRef]
11. Lekas, E.; Johansson, M.; Widmark, A.; Bergh, A.; Damber, J.E. Decrement of blood flow precedes the involution of the ventral prostate in the rat after castration. *Urol. Res.* **1997**, *25*, 309–314. [CrossRef] [PubMed]
12. Kalmuk, J.; Folaron, M.; Buchinger, J.; Pili, R.; Seshadri, M. Multimodal imaging guided preclinical trials of vascular targeting in prostate cancer. *Oncotarget* **2015**, *6*, 24376–24392. [CrossRef] [PubMed]

13. Roe, K.; Mikalsen, L.T.; van der Kogel, A.J.; Bussink, J.; Lyng, H.; Ree, A.H.; Marignol, L.; Olsen, D.R. Vascular responses to radiotherapy and androgen-deprivation therapy in experimental prostate cancer. *Radiat. Oncol.* **2012**, *7*, 75. [CrossRef]
14. Johansson, A.; Rudolfsson, S.H.; Kilter, S.; Bergh, A. Targeting castration-induced tumour hypoxia enhances the acute effects of castration therapy in a rat prostate cancer model. *BJU Int.* **2011**, *107*, 1818–1824. [CrossRef]
15. Franck-Lissbrant, I.; Haggstrom, S.; Damber, J.E.; Bergh, A. Testosterone stimulates angiogenesis and vascular regrowth in the ventral prostate in castrated adult rats. *Endocrinology* **1998**, *139*, 451–456. [CrossRef] [PubMed]
16. Shabsigh, A.; Ghafar, M.A.; de la Taille, A.; Burchardt, M.; Kaplan, S.A.; Anastasiadis, A.G.; Buttyan, R. Biomarker analysis demonstrates a hypoxic environment in the castrated rat ventral prostate gland. *J. Cell Biochem.* **2001**, *81*, 437–444. [CrossRef] [PubMed]
17. Lejeune, F.J.; Lienard, D.; Matter, M.; Ruegg, C. Efficiency of recombinant human TNF in human cancer therapy. *Cancer Immun.* **2006**, *6*, 6.
18. Petrache, I.; Verin, A.D.; Crow, M.T.; Birukova, A.; Liu, F.; Garcia, J.G. Differential effect of MLC kinase in TNF-alpha-induced endothelial cell apoptosis and barrier dysfunction. *Am. J. Physiol. Lung Cell Mol. Physiol.* **2001**, *280*, L1168–L1178. [CrossRef]
19. Watson, P.A.; Ellwood-Yen, K.; King, J.C.; Wongvipat, J.; Lebeau, M.M.; Sawyers, C.L. Context-dependent hormone-refractory progression revealed through characterization of a novel murine prostate cancer cell line. *Cancer Res.* **2005**, *65*, 11565–11571. [CrossRef]
20. Ellis, L.; Lehet, K.; Ramakrishnan, S.; Adelaiye, R.; Miles, K.M.; Wang, D.; Liu, S.; Atadja, P.; Carducci, M.A.; Pili, R. Concurrent HDAC and mTORC1 inhibition attenuate androgen receptor and hypoxia signaling associated with alterations in microRNA expression. *PLoS ONE* **2011**, *6*, e27178. [CrossRef]
21. Wang, S.; Gao, J.; Lei, Q.; Rozengurt, N.; Pritchard, C.; Jiao, J.; Thomas, G.V.; Li, G.; Roy-Burman, P.; Nelson, P.S.; et al. Prostate-specific deletion of the murine Pten tumor suppressor gene leads to metastatic prostate cancer. *Cancer Cell* **2003**, *4*, 209–221. [CrossRef]
22. Singh, S.; Pan, C.; Wood, R.; Yeh, C.R.; Yeh, S.; Sha, K.; Krolewski, J.J.; Nastiuk, K.L. Quantitative volumetric imaging of normal, neoplastic and hyperplastic mouse prostate using ultrasound. *BMC Urol.* **2015**, *15*, 97. [CrossRef] [PubMed]
23. Pan, C.; Singh, S.; Sahasrabudhe, D.M.; Chakkalakal, J.V.; Krolewski, J.J.; Nastiuk, K.L. TGFbeta Superfamily Members Mediate Androgen Deprivation Therapy-Induced Obese Frailty in Male Mice. *Endocrinology* **2016**, *157*, 4461–4472. [CrossRef] [PubMed]
24. Rich, L.J.; Seshadri, M. Photoacoustic monitoring of tumor and normal tissue response to radiation. *Sci. Rep.* **2016**, *6*, 21237. [CrossRef] [PubMed]
25. Rich, L.J.; Seshadri, M. Photoacoustic imaging of vascular hemodynamics: Validation with blood oxygenation level-dependent MR imaging. *Radiology* **2015**, *275*, 110–118. [CrossRef]
26. Ellwood-Yen, K.; Graeber, T.G.; Wongvipat, J.; Iruela-Arispe, M.L.; Zhang, J.; Matusik, R.; Thomas, G.V.; Sawyers, C.L. Myc-driven murine prostate cancer shares molecular features with human prostate tumors. *Cancer Cell* **2003**, *4*, 223–238. [CrossRef]
27. Gurel, B.; Iwata, T.; Koh, C.M.; Jenkins, R.B.; Lan, F.; Van Dang, C.; Hicks, J.L.; Morgan, J.; Cornish, T.C.; Sutcliffe, S.; et al. Nuclear MYC protein overexpression is an early alteration in human prostate carcinogenesis. *Mod. Pathol.* **2008**, *21*, 1156–1167. [CrossRef]
28. Maolake, A.; Zhang, R.; Sha, K.; Singh, S.; Pan, C.; Xu, B.; Chatta, G.; Mastri, M.; Eng, K.H.; Krolewski, J.J.; et al. Glucocorticoid signaling delays castration-induced regression in murine models of prostate cancer. *BioRxiv* **2022**. [CrossRef]
29. Goertz, D.E.; Yu, J.L.; Kerbel, R.S.; Burns, P.N.; Foster, F.S. High-frequency Doppler ultrasound monitors the effects of antivascular therapy on tumor blood flow. *Cancer Res.* **2002**, *62*, 6371–6375.
30. Hamper, U.M.; DeJong, M.R.; Caskey, C.I.; Sheth, S. Power Doppler imaging: Clinical experience and correlation with color Doppler US and other imaging modalities. *Radiographics* **1997**, *17*, 499–513. [CrossRef]
31. Choi, B.I.; Kim, T.K.; Han, J.K.; Chung, J.W.; Park, J.H.; Han, M.C. Power versus conventional color Doppler sonography: Comparison in the depiction of vasculature in liver tumors. *Radiology* **1996**, *200*, 55–58. [CrossRef] [PubMed]
32. Tomaszewski, M.R.; Gonzalez, I.Q.; O'Connor, J.P.; Abeyakoon, O.; Parker, G.J.; Williams, K.J.; Gilbert, F.J.; Bohndiek, S.E. Oxygen Enhanced Optoacoustic Tomography (OE-OT) Reveals Vascular Dynamics in Murine Models of Prostate Cancer. *Theranostics* **2017**, *7*, 2900–2913. [CrossRef] [PubMed]
33. Armenia, J.; Wankowicz, S.A.M.; Liu, D.; Gao, J.; Kundra, R.; Reznik, E.; Chatila, W.K.; Chakravarty, D.; Han, G.C.; Coleman, I.; et al. The long tail of oncogenic drivers in prostate cancer. *Nat. Genet.* **2018**, *50*, 645–651. [CrossRef] [PubMed]
34. Barnett, C.M.; Heinrich, M.C.; Lim, J.; Nelson, D.; Beadling, C.; Warrick, A.; Neff, T.; Higano, C.S.; Garzotto, M.; Qian, D.; et al. Genetic profiling to determine risk of relapse-free survival in high-risk localized prostate cancer. *Clin. Cancer Res.* **2014**, *20*, 1306–1312. [CrossRef]
35. Luo, Y.; Azad, A.K.; Karanika, S.; Basourakos, S.P.; Zuo, X.; Wang, J.; Yang, L.; Yang, G.; Korentzelos, D.; Yin, J.; et al. Enzalutamide and CXCR7 inhibitor combination treatment suppresses cell growth and angiogenic signaling in castration-resistant prostate cancer models. *Int. J. Cancer* **2018**, *142*, 2163–2174. [CrossRef]
36. Miyata, Y.; Mitsunari, K.; Asai, A.; Takehara, K.; Mochizuki, Y.; Sakai, H. Pathological significance and prognostic role of microvessel density, evaluated using CD31, CD34, and CD105 in prostate cancer patients after radical prostatectomy with neoadjuvant therapy. *Prostate* **2015**, *75*, 84–91. [CrossRef]
37. Naito, H.; Iba, T.; Wakabayashi, T.; Tai-Nagara, I.; Suehiro, J.I.; Jia, W.; Eino, D.; Sakimoto, S.; Muramatsu, F.; Kidoya, H.; et al. TAK1 Prevents Endothelial Apoptosis and Maintains Vascular Integrity. *Dev. Cell* **2019**, *48*, 151–166.e7. [CrossRef]

38. Clauss, M.; Sunderkotter, C.; Sveinbjornsson, B.; Hippenstiel, S.; Willuweit, A.; Marino, M.; Haas, E.; Seljelid, R.; Scheurich, P.; Suttorp, N.; et al. A permissive role for tumor necrosis factor in vascular endothelial growth factor-induced vascular permeability. *Blood* **2001**, *97*, 1321–1329. [CrossRef]
39. Gao, S.; Lee, P.; Wang, H.; Gerald, W.; Adler, M.; Zhang, L.; Wang, Y.F.; Wang, Z. The androgen receptor directly targets the cellular Fas/FasL-associated death domain protein-like inhibitory protein gene to promote the androgen-independent growth of prostate cancer cells. *Mol. Endocrinol.* **2005**, *19*, 1792–1802. [CrossRef]
40. Nastiuk, K.L.; Kim, J.W.; Mann, M.; Krolewski, J.J. Androgen regulation of FLICE-like inhibitory protein gene expression in the rat prostate. *J. Cell Physiol.* **2003**, *196*, 386–393. [CrossRef]
41. Nastiuk, K.L.; Krolewski, J.J. FLIP-ping out: Death receptor signaling in the prostate. *Cancer Biol. Ther.* **2008**, *7*, 1171–1179. [CrossRef]
42. Prins, G.S.; Birch, L.; Greene, G.L. Androgen receptor localization in different cell types of the adult rat prostate. *Endocrinology* **1991**, *129*, 3187–3199. [CrossRef] [PubMed]
43. Wu, J.; Hadoke, P.W.; Takov, K.; Korczak, A.; Denvir, M.A.; Smith, L.B. Influence of Androgen Receptor in Vascular Cells on Reperfusion following Hindlimb Ischaemia. *PLoS ONE* **2016**, *11*, e0154987. [CrossRef] [PubMed]
44. Graeber, T.G.; Peterson, J.F.; Tsai, M.; Monica, K.; Fornace, A.J., Jr.; Giaccia, A.J. Hypoxia induces accumulation of p53 protein, but activation of a G1-phase checkpoint by low-oxygen conditions is independent of p53 status. *Mol. Cell Biol.* **1994**, *14*, 6264–6277.
45. Colombel, M.; Radvanyi, F.; Blanche, M.; Abbou, C.; Buttyan, R.; Donehower, L.A.; Chopin, D.; Thiery, J.P. Androgen suppressed apoptosis is modified in p53 deficient mice. *Oncogene* **1997**, *10*, 1269–1274.
46. Berges, R.R.; Furuya, Y.; Remington, L.; English, H.F.; Jacks, T.; Isaacs, J.T. Cell proliferation, DNA repair, and p53 function are not required for programmed death of prostatic glandular cells induced by androgen ablation. *Proc. Natl. Acad. Sci. USA* **1993**, *90*, 8910–8914. [CrossRef]
47. Sermeus, A.; Michiels, C. Reciprocal influence of the p53 and the hypoxic pathways. *Cell Death Dis.* **2011**, *2*, e164. [CrossRef] [PubMed]
48. Leszczynska, K.B.; Foskolou, I.P.; Abraham, A.G.; Anbalagan, S.; Tellier, C.; Haider, S.; Span, P.N.; O'Neill, E.E.; Buffa, F.M.; Hammond, E.M. Hypoxia-induced p53 modulates both apoptosis and radiosensitivity via AKT. *J. Clin. Investig.* **2015**, *125*, 2385–2398. [CrossRef] [PubMed]
49. Folli, S.; Pelegrin, A.; Chalandon, Y.; Yao, X.; Buchegger, F.; Lienard, D.; Lejeune, F.; Mach, J.P. Tumor-necrosis factor can enhance radio-antibody uptake in human colon carcinoma xenografts by increasing vascular permeability. *Int. J. Cancer* **1993**, *53*, 829–836. [CrossRef]
50. Longo, D.L.; Stefania, R.; Callari, C.; De Rose, F.; Rolle, R.; Conti, L.; Consolino, L.; Arena, F.; Aime, S. Water Soluble Melanin Derivatives for Dynamic Contrast Enhanced Photoacoustic Imaging of Tumor Vasculature and Response to Antiangiogenic Therapy. *Adv. Healthc. Mater.* **2017**, *18*, 1719. [CrossRef]
51. Royall, J.A.; Berkow, R.L.; Beckman, J.S.; Cunningham, M.K.; Matalon, S.; Freeman, B.A. Tumor necrosis factor and interleukin 1 alpha increase vascular endothelial permeability. *Am. J. Physiol.* **1989**, *257 Pt 1*, L399–L410. [CrossRef] [PubMed]
52. Kallinowski, F.; Schaefer, C.; Tyler, G.; Vaupel, P. In vivo targets of recombinant human tumour necrosis factor-alpha: Blood flow, oxygen consumption and growth of isotransplanted rat tumours. *Br. J. Cancer* **1989**, *60*, 555–560. [CrossRef] [PubMed]
53. Balkwill, F.R.; Naylor, M.S.; Malik, S. Tumour necrosis factor as an anticancer agent. *Eur. J. Cancer* **1990**, *26*, 641–644. [CrossRef] [PubMed]
54. Curnis, F.; Sacchi, A.; Borgna, L.; Magni, F.; Gasparri, A.; Corti, A. Enhancement of tumor necrosis factor alpha antitumor immunotherapeutic properties by targeted delivery to aminopeptidase N (CD13). *Nat. Biotechnol.* **2000**, *18*, 1185–1190. [CrossRef]
55. Bertilaccio, M.T.; Grioni, M.; Sutherland, B.W.; Degl'Innocenti, E.; Freschi, M.; Jachetti, E.; Greenberg, N.M.; Corti, A.; Bellone, M. Vasculature-targeted tumor necrosis factor-alpha increases the therapeutic index of doxorubicin against prostate cancer. *Prostate* **2008**, *68*, 1105–1115. [CrossRef]
56. Probst, P.; Stringhini, M.; Ritz, D.; Fugmann, T.; Neri, D. Antibody-based Delivery of TNF to the Tumor Neovasculature Potentiates the Therapeutic Activity of a Peptide Anticancer Vaccine. *Clin. Cancer Res.* **2019**, *25*, 698–709. [CrossRef]

656 **Supplementary Figures**

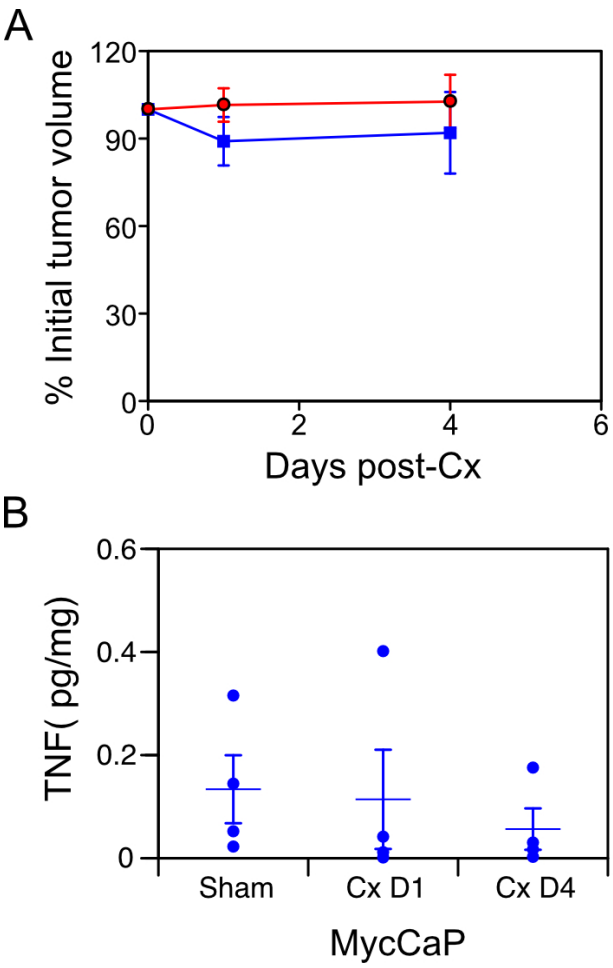

Supplementary Figure S1. Tumor volume and TNF protein levels were not changed post-castration in prostate cancer allografts. A, HFUS determined Myc-CaP tumor volume after castration (normalized to pre-castration volume) in mice treated with vehicle (n=9, blue) or sTNFR2-Fc (n = 7, red). **B,** Tumor tissue was collected from FVB mice bearing Myc-CaP subcutaneous xenografts one and four days after castration (Cx) or from sham-castrated mice. TNF protein levels were measured in solubilized tumor tissue by ELISA (R&D #DY410), pg per mg soluble tumor extract, n = 4 tumors for each group, with individual tumor TNF quantities (circles), and group means (lines) and SEM (bars).

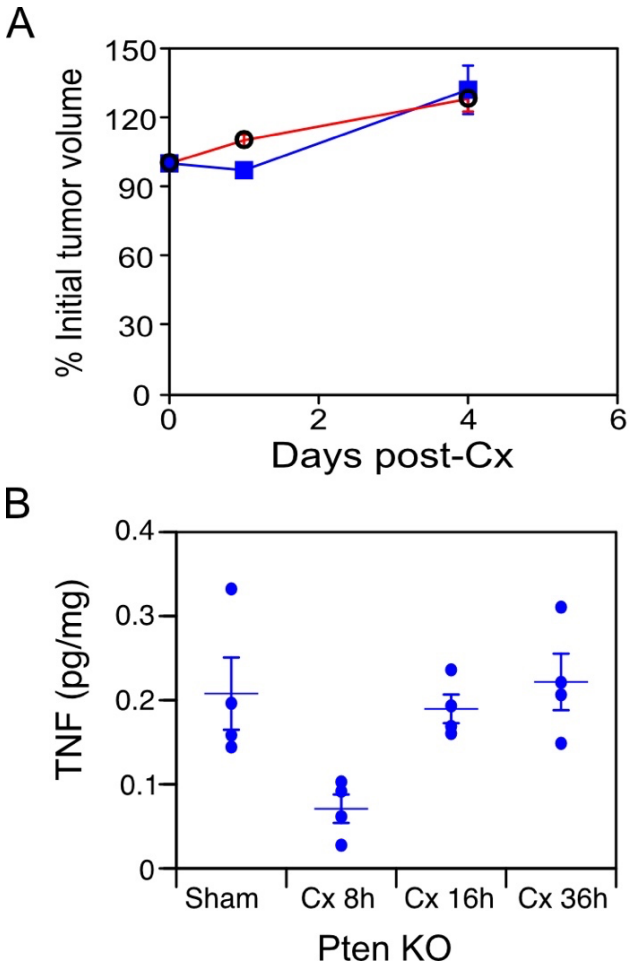

Supplemental Figure S2. Tumor volume and TNF protein levels are not changed post-castration in autochthonous prostate cancers. A, HFUS determined tumor volume post-castration (normalized to pre-castration) in PbCre4 x Pten$^{fl/fl}$ mice treated with vehicle (n=4, blue) or sTNFR2-Fc (n = 4, red). **B,** Tumor tissue was collected from PbCre4 x Pten$^{fl/fl}$ mice at the indicated time (in hours) after castration (Cx) or from sham-castrated mice. TNF protein levels by ELISA, n = 4 tumors for each group, with individual tumor TNF quantities (circles), and group means (lines) and SEM (bars).

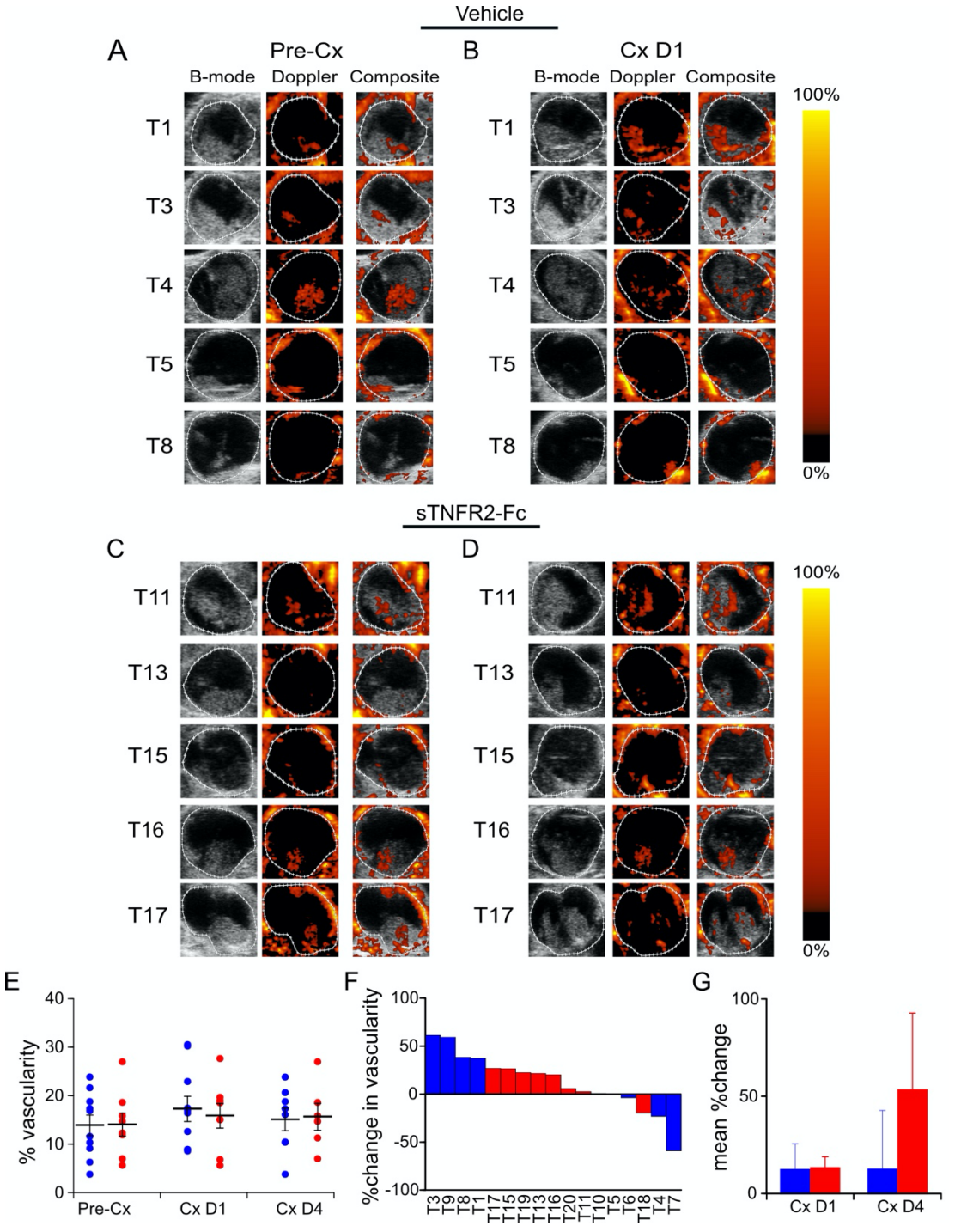

Supplementary Figure S3. Castration does not alter blood flow in prostate tumors of PbCre4 x Ptenfl/fl mice. **A,** Power Doppler (PD) images of subcutaneous PTEN KO tumors pre-castration (Pre-Cx) of mice treated with PBS (Vehicle), 5 tumors (of 10 evaluable tumors) are shown. Left to right: Gray-scale ultrasound image (B-mode); PD pseudo-colored image (Doppler); Composite of pseudo-colored PD image overlaid on the B-mode image (Composite). **B,** PD images of tumors in panel A, one day after castration (Cx D1). **C,** PD images of a second set of PTEN KO tumors pre-castration (Pre-Cx) of mice treated with sTNFR2-Fc, tumors 11, 13, 15, 15 (of 8 evaluable tumors). Images as described in A. **D,** PD images of PTEN tumors one day after castration (Cx D1) of mice treated with sTNFR2-Fc. Images as described in A. **E,** PD signal (% vascularity) from tumors in vehicle treated mice (blue) or tumors in sTNFR2-Fc treated mice (red) pre-castration, and at one and four days after castration. **F,** Waterfall plot of %change in vascularity in individual tumors one day after castration. **G,** Mean %change in paired measures of vascularity pre-castration versus Cx D1 (n = 9 evaluable tumors from vehicle-treated mice; n = 8 from sTNFRII-Fc treated mice) or Cx D4 (n = 7, 5, respectively). Mean (columns) and SEM (bars).

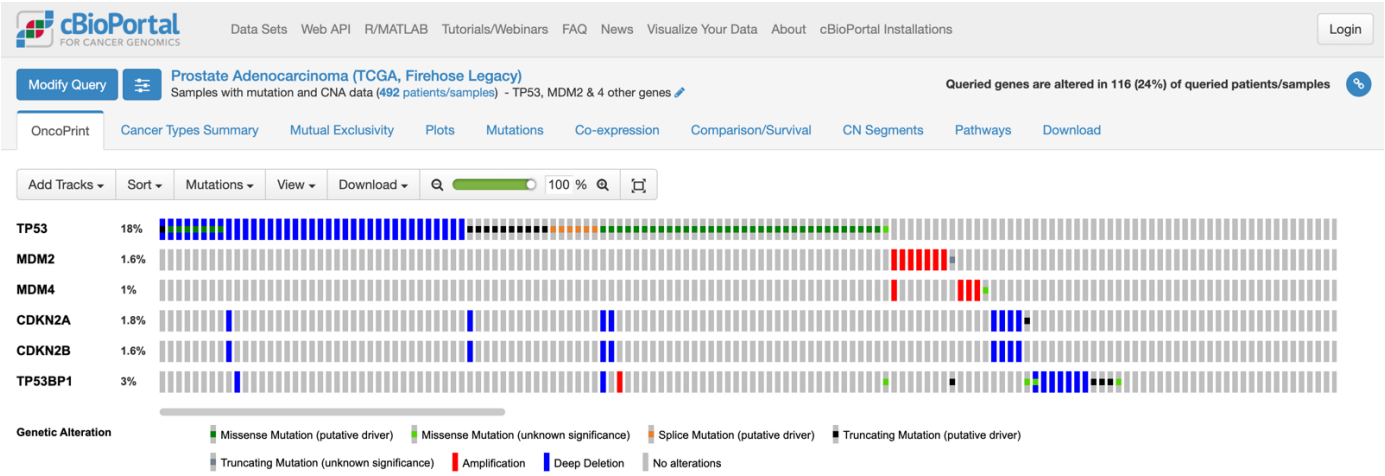

Supplementary Figure S4. TP53 mutation frequency in primary prostate cancers. OncoPrint depiction of cBioPortal analysis of genomic alterations (mutations and copy number alterations) of TP53 and related genes in the TCGA dataset (TCGA, Firehouse Legacy) containing 492 primary prostate cancers. The key indicates the color-coding of the alterations. Grey bars have no alterations for the indicated set of 6 genes. Only a portion of the unaltered patient cases are shown.